The Astrophysical Journal, 769:85 (15pp), 2013 June 1 doi:10.1088/0004-637X/769/2/85

GRB060218 AS A TIDAL DISRUPTION OF A WHITE DWARF BY AN INTERMEDIATE-MASS BLACK HOLE

Roman V. Shcherbakov[1,2,7], Asaf Pe'er[3,4], Christopher S. Reynolds[1,2], Roland Haas[5,6], Tanja Bode[6], and Pablo Laguna[6]

[1] Department of Astronomy, University of Maryland, College Park, MD 20742, USA
[2] Joint Space Science Institute, University of Maryland, College Park, MD 20742, USA
[3] Harvard-Smithsonian Center for Astrophysics, 60 Garden Street, Cambridge, MA 02138, USA
[4] Department of Physics, University College Cork, Cork, Ireland
[5] Theoretical AstroPhysics Including Relativity, California Institute of Technology, Pasadena, CA 91125, USA
[6] Center for Relativistic Astrophysics, School of Physics, Georgia Institute of Technology, Atlanta, GA 30332, USA

Received 2012 December 13; accepted 2013 March 18; published 2013 May 7

ABSTRACT

The highly unusual pair of a gamma-ray burst (GRB) GRB060218 and an associated supernova, SN2006aj, has puzzled theorists for years. A supernova shock breakout and a jet from a newborn stellar mass compact object have been proposed to explain this pair's multiwavelength signature. Alternatively, we propose that the source is naturally explained by another channel: the tidal disruption of a white dwarf (WD) by an intermediate-mass black hole (IMBH). This tidal disruption is accompanied by a tidal pinching, which leads to the ignition of a WD and a supernova. Some debris falls back onto the IMBH, forms a disk, which quickly amplifies the magnetic field, and launches a jet. We successfully fit soft X-ray spectra with the Comptonized blackbody emission from a jet photosphere. The optical/UV emission is consistent with self-absorbed synchrotron emission from the expanding jet front. The temporal dependence of the accretion rate $\dot{M}(t)$ in a tidal disruption provides a good fit to the soft X-ray light curve. The IMBH mass is found to be about $10^4\,M_\odot$ in three independent estimates: (1) fitting the tidal disruption $\dot{M}(t)$ to the soft X-ray light curve, (2) computing the jet base radius in a jet photospheric emission model, and (3) inferring the mass of the central black hole based on the host dwarf galaxy's stellar mass. The position of the supernova is consistent with the center of the host galaxy, while the low supernova ejecta mass is consistent with that of a WD. The high expected rate of tidal disruptions in dwarf galaxies is consistent with one source observed by the *Swift* satellite over several years at a distance of 150 Mpc measured for GRB060218. Encounters with WDs provide much fuel for the growth of IMBHs.

Key words: accretion, accretion disks – black hole physics – radiation mechanisms: general – supernovae: general – X-rays: bursts – X-rays: individual (GRB060218)

Online-only material: color figures

1. INTRODUCTION

The existence of stellar mass black holes (BHs) with masses $M_{\rm BH} < 100\,M_\odot$ and supermassive black holes (SMBHs) with masses $M_{\rm BH} > 10^5\,M_\odot$ has long been established. A population of intermediate-mass black holes (IMBHs) likely exists. These BHs have masses in the range $100\,M_\odot < M_{\rm BH} < 10^5\,M_\odot$. They may live in the centers of dwarf galaxies (Dong et al. 2007; Greene 2012) or globular clusters (GCs; Fabbiano et al. 1997, 2001; Colbert & Mushotzky 1999; Matsumoto et al. 2001; Gültekin et al. 2004). The IMBHs may form via the collapse of a massive cloud (Begelman et al. 2006) or a massive star (Fryer et al. 2001; Madau & Rees 2001; Schneider et al. 2002) or they may grow from a stellar mass BH. A star cluster G1 in the M31 galaxy is estimated to host a $2\times10^4\,M_\odot$ BH (Gebhardt et al. 2002) based on its velocity dispersion profile. The SDSS J160531.84+174826.1 dwarf galaxy is estimated to have an IMBH with a mass of $\sim7\times10^4\,M_\odot$ based on luminosity scaling relations (Dong et al. 2007). One of the best candidates is the HLX-1 source in the ESO 243-49 galaxy. The estimated BH mass is $3\times10^4\,M_\odot$ based on a thin disk thermal state (Davis et al. 2011). All of the candidates mentioned are still tentative and the uncertainty of the mass estimates is up to an order of magnitude. More IMBH candidates with qualitatively different observational signatures may provide stronger evidence for the existence of such objects.

Tidal disruptions of white dwarfs (WDs) by IMBHs provide such qualitatively different signatures. Unlike disruptions of main-sequence (MS) stars, which happen far away from the BHs and have slow timescales, the disruptions of WDs are very fast. Such disruptions may lead to accretion rates up to $10^4\,M_\odot\,{\rm yr}^{-1}$ (Haas et al. 2012). A flow with an extreme accretion rate may produce a short powerful burst of radiation, for example, when a jet is launched. The X-ray emission of the Swift J1644+57 source is attributed to a jet launched by a super-Eddington accretion disk formed after a tidal disruption of a star by a SMBH (Bloom et al. 2011; Burrows et al. 2011; Levan et al. 2011; Zauderer et al. 2011). An alternative theory (Krolik & Piran 2011) ascribes Swift J1644+57 to an encounter of a WD with an IMBH.

When particle acceleration is inefficient, then the only radiation from the jet is photospheric emission (Eichler & Levinson 2000; Mészáros & Rees 2000; Daigne & Mochkovitch 2002; Rees & Mészáros 2005). The radiation field is in thermal equilibrium with matter within a dense hot jet up to the distance $R_{\rm ph}$ along the jet, called the photospheric radius, where the optical depth to Compton scattering is about unity $\tau_\sigma \sim 1$. The photospheric emission has a quasi-blackbody spectrum (Pe'er et al. 2007; Pe'er 2008; Pe'er & Ryde 2011; Beloborodov 2011). Particle acceleration may happen either in the entire volume of the

[7] Hubble Fellow.

jet or in the internal shocks. Dissipation in the volume of the jet, in particular in the sub-photospheric regions, leads to a modified blackbody spectrum from near the jet photosphere (Pe'er et al. 2005, 2006; Giannios 2006, 2012). Modifications include the Comptonization and the broadening of the blackbody peak with pair production. Effective particle acceleration in the internal shocks (Meszaros 2006) is likely responsible for the emission of gamma-ray bursts (GRBs). When two shells moving at different speeds collide above the photosphere, a shock forms, and a substantial fraction of relative kinetic energy can be transferred into the electrons (Rees & Meszaros 1994; Sari & Piran 1997), which radiate synchrotron emission. The collisions of shells are especially efficient when the jet bulk Lorentz factor Γ is large. For small Lorentz factors and large photospheric radii, such as in the jets from tidal disruptions of the WDs by the IMBHs, the collisions of shells may happen within the photosphere, and the internal shock signatures might be weaker. The fluctuations of the jet Γ diffuse out, while the jet travels within the photosphere, and the fluctuations outside of the photosphere are small. Even when the slow shells collide, the energy release is weak. Therefore, we expect to see a strong blackbody signature of photospheric emission. While the energy density of the slow tidal disruption jet might not warrant fast pair production, the Comptonization is still expected to modify the spectrum.

A distinct feature of WD disruptions by IMBHs is a supernova. As a consequence of the tidal compression along the angular momentum axis, a WD may undergo thermonuclear ignition (Luminet 1985; Luminet & Marck 1985; Luminet & Pichon 1989b) and explode. The energy and the composition of the resulting supernova are functions of the WD mass $m_{\rm WD}$, the pericenter radius R_P, and the BH mass $M_{\rm BH}$ (Rosswog et al. 2009). If the WD is massive and the disruption is deep, then the explosion could be similar to a Type Ia supernova with a comparable energy release. Less massive WDs may lead to low-luminosity explosions with little Ni synthesized. There is no explosion at all in some cases. In any case the ejected mass of $\lesssim 1\ M_\odot$ is less than that in core-collapse supernovae.

In sum, we predict a transient similar to a GRB, but softer and longer, accompanied by a supernova with a small ejecta mass. The best candidate we find in the *Swift* GRB catalog is the source GRB060218. This unusual event is an underluminous very long GRB with a duration of $t_{90} \approx 2600$ s and with a smooth X-ray light curve (Soderberg et al. 2006). It is accompanied by a fast supernova, SN2006aj, which was modeled to have a low ejecta mass $M_{\rm ej} \sim 1$–$2\ M_\odot$ (Mazzali et al. 2006a). The X-ray emission has a blackbody component characteristic of photospheric radiation. The early X-ray radiation is accompanied by powerful optical/UV emission (Ghisellini et al. 2007a). Two classes of theories were proposed to explain the source: a supernova shock breakout model (Campana et al. 2006; Waxman et al. 2007; Nakar & Sari 2012) and a model with a mildly relativistic jet from a newborn compact object such as a magnetar (Fan et al. 2006; Toma et al. 2007; Ghisellini et al. 2007a, 2007b). Nevertheless, we think that a tidal disruption of a WD by an IMBH is not only a viable model for the source but also more naturally explains some features such as duration and the soft quasi-thermal spectrum.

The paper is organized as follows. In Section 2, we describe in more detail the observations of GRB060218/SN2006aj. We extensively discuss in Section 3 the former theoretical explanations of the source: the shock breakout model and a jet launched by a newborn compact object. Then in Section 4 we concentrate on modeling within a tidal disruption scenario. We re-derive the dynamics of a tidal disruption and discuss the physics of jet launching. We perform time-resolved spectroscopy of the source and successfully model the X-ray emission with a Comptonized blackbody spectrum from the photosphere. The derived jet base radius corresponds to about $10^4\ M_\odot$ IMBH. We propose that the origin of the powerful early optical/UV radiation is the front region of a propagating jet. We find that the full X-ray light curve can be fitted well by a scaled dependence of the fallback accretion rate on time $\dot{M}(t)$. The fit provides an IMBH mass of about $10^4\ M_\odot$. We find that the steep decay phase is consistent with the action of absorption alone and that the afterglow can be naturally explained as powered by the central engine operating in a shallow $t^{-4/3}$ regime. The associated supernova is consistent with a WD origin, while its position is consistent with the center of a host galaxy. The mass of the dwarf host galaxy provides an estimate of a central IMBH mass of about $10^4\ M_\odot$. In Section 5, we estimate the event rates. A high rate of tidal disruptions is predicted in the dwarf galaxies, while the disruptions of the WDs constitute a significant percentage of all disruptions. Since the disruptions of the MS stars mostly happen at large distances from the BHs, then such events could be much dimmer than the disruptions of the WDs. The tidal disruptions of the WDs provide plenty of material to feed the central IMBH up to a supermassive size.

2. OBSERVATIONS OF GRB060218

GRB060218 triggered the Burst Alert Telescope (BAT) on board the *Swift* mission satellite on 2006 February 18 (Campana et al. 2006). Soon after the trigger the X-ray Telescope (XRT) identified a bright source whose count rate peaked at around 960 s from the initial trigger of the BAT. Then the source gradually decayed over a continuous observation period, which ended at around 2700 s. The event duration $t_{90} = 2600$ s is unusually long for a *Swift* GRB (Campana et al. 2006), and the XRT light curve was unusually smooth and regular. The rise period is characterized by hard emission with a BAT flux about equal to the XRT flux (Campana et al. 2006; Toma et al. 2007) and with a peak energy $E_p \sim 5$ keV. The isotropic-equivalent luminosity is $L_{\rm iso} \sim 10^{47}$ erg s^{-1}, which is about 10^5 times less than for typical GRBs (Toma et al. 2007). The source is found to have a blackbody component with a low temperature $T \sim 0.2$ keV, whose flux contribution increased with time from 15% to 80% (Campana et al. 2006; Li 2007). The *Swift* satellite returned to observe the source at ~6000 s and found it in a steep decay phase with the absorbed flux ~100 times below the peak value. After about 1.5×10^4 s the decay of the X-ray flux flattened into a shallow afterglow with an X-ray luminosity $L_X \propto t^{-1.2}$ (Soderberg et al. 2006). Simultaneous observations by the Ultra-Violet/Optical Telescope (UVOT) on board the *Swift* satellite revealed substantial early emission peaking at about 5×10^4 s with a dereddened UV flux $\nu F_\nu \sim 10^{-10}$ erg s^{-1} cm^{-2} (Ghisellini et al. 2007a). A lower peak at a level of $\nu F_\nu \approx 6 \times 10^{-12}$ erg s^{-1} cm^{-2} followed after several days. The second peak is attributed to a supernova SN2006aj (Maeda et al. 2007; Mazzali et al. 2006a; Modjaz et al. 2006; Pian et al. 2006), while the origin of the first peak is debated (Waxman et al. 2007; Ghisellini et al. 2007a, 2007b).

The supernova was classified as Type Ic (Mazzali et al. 2006a). However, its unique spectral properties prompted researchers to suggest a new Type Id classification (Mazzali et al. 2006a; Maeda et al. 2007). The rapid supernova peaked at 10 days (Pian et al. 2006), which is the fastest of all

supernovae associated with GRBs (Ferrero et al. 2006). According to Mazzali et al. (2007, p. 5), "the ejected mass predicted below 8000 km s^{-1} by the model used by Mazzali et al. (2006a) is $M_{ej} = 1\,M_\odot$," while the nebular phase observations suggest a higher total ejecta mass, $M_{ej} = 2\,M_\odot$ (Mazzali et al. 2006a, 2007; Maeda et al. 2007). The estimated ^{56}Ni mass in the ejecta is $0.2\,M_\odot$. The ejecta consists mostly of oxygen and carbon (Mazzali et al. 2007), but also contains some silicon and iron (Mirabal et al. 2006). The correspondent supernova energy is $E_K \sim 2 \times 10^{51}$ erg. Both the ejecta mass and total energy are much less than the typical ejecta mass $M_{ej} = 10\,M_\odot$ and the typical energy $E_K = 3 \times 10^{52}$ erg, for GRB-supernovae (see Mazzali et al. 2006a and references therein). Substantial optical polarization (Gorosabel et al. 2006) indicates an asymmetry of the ejected material.

The optical observations of the host galaxy indicate a source redshift $z = 0.0335$ (Mirabal et al. 2006; Modjaz et al. 2006), which corresponds to a distance $d = 143$ Mpc. GRB060218 is associated with a dwarf star-forming galaxy with a stellar mass $M_{st} \sim 10^{7.2}\,M_\odot$ (Ferrero et al. 2007), a metallicity $Z \approx 0.07\,Z_\odot$ (Wiersema et al. 2007), and a characteristic radius $R_{80} = 0.55$ kpc (Svensson et al. 2010). The supernova and the host galaxy were observed by the *Hubble Space Telescope* (*HST*) Advanced Camera for Surveys (ACS) instrument under the program GO 10551 (PI: Kulkarni) in cycle 14. The images produced by Misra et al. (2011) reveal some irregularity of the host dwarf galaxy morphology.

3. FORMER THEORETICAL MODELS

GRB060218 and its associated supernova SN2006aj sparked substantial interest among researchers with over 10 papers being dedicated to the theoretical explanations of this highly unusual source. Theoretical efforts can be divided into two major categories: a shock breakout model and a model with a jet launched by a magnetar or by a stellar-mass BH. In the following subsections, we briefly review the theoretical models emphasizing some successful applications of the models as well as their problems. In the following section, we offer an explanation of the source within the tidal disruption scenario.

3.1. Shock Breakout Model

The shock breakout model states that a nuclear explosion following the collapse of a massive core launches a shock wave, which propagates out through the star (Colgate 1968). The radiation-dominated shock deposits its energy into the low-density gas at the stellar surface (Katz et al. 2010). The heated gas radiates bremsstrahlung photons, which are inverse-Compton-scattered into the X-ray and γ-ray bands. The shock deposits up to 10^{48} erg of energy, most of which is radiated as an X-ray flash (Colgate 1974). A variety of sources were successfully explained with the supernova shock breakout model. A good example of this is XRF080109 and its associated Type Ib/c supernova SN2008D. The large supernova ejecta mass for this source, $M_{ej} = 4$–$7\,M_\odot$ (Soderberg et al. 2008; Mazzali et al. 2008), and the low X-ray radiation energy, 10^{45}–10^{46} erg (Chevalier & Fransson 2008), leave little doubt as to its shock breakout origin. Other sources that fit this model include the X-ray brightening of supernova SNLS-04D2dc (Schawinski et al. 2008) with low X-ray-radiated energy, $\leqslant 10^{47}$ erg, SN1998bw with an ejecta mass of $\sim 12\,M_\odot$ accompanied by XRF/GRB980425 (Woosley et al. 1999), and SN2003lw with an ejecta mass of $13\,M_\odot$ accompanied by the weak XRF/GRB031203 (Mazzali et al. 2006b).

In the case of XRF060218, the deposited energy of $10^{49.5}$ erg is quite large (Campana et al. 2006). The peak isotropic unabsorbed flux of the soft X-ray component is $F_{BB} = (3$–$6) \times 10^{-8}$ erg s^{-1} cm^{-2} with a temperature $T_{BB} = 0.11$–0.17 keV (Butler 2007). These parameters correspond to blackbody emission from the non-relativistic medium at a radius $R = (3$–$8) \times 10^{12}$ cm, while Campana et al. (2006) inferred $R = (0.5$–$1) \times 10^{12}$ cm within their analysis at early times and $R = (0.2$–$2) \times 10^{12}$ cm at late times. This radius indicates a compact progenitor such as a Wolf–Rayet (WR) star. Large explosion energy might be inconsistent with non-relativistic expansion. A mildly relativistic ejecta velocity of $v \approx 0.85c$ was proposed in later modeling by Waxman et al. (2007), who also stated that the emission should come from the photosphere above the stellar surface. The relativistic shock breakout theory was further developed by Nakar & Sari (2012), who computed the shock dynamics, the light curve, and the spectrum. The spectrum is predicted to be quasi-thermal with a temperature around 50 keV. Nakar & Sari (2012) derived a relation between the XRF event duration, the total energy, and the observed temperature,

$$t_{bo} \sim 20\ \mathrm{s} \left(\frac{E_{bo}}{10^{46}\ \mathrm{erg}}\right)^{1/2} \left(\frac{T_{bo}}{50\ \mathrm{keV}}\right)^{-2.68}. \quad (1)$$

To satisfy this relation, the early temperature of 40 keV is taken for GRB060218 consistent with the peak energy 36 keV at very early times (Toma et al. 2007).

The shock breakout theory has its problems. For instance, Li (2007) concluded that the observed temperature and the total energy of GRB060218 lead to an unrealistically large photospheric radius R_{ph} inconsistent with that of the galactic WR stellar population. This conclusion is strengthened by our larger estimate of the emission radius. The large R_{ph} in the model by Nakar & Sari (2012) corresponds to an unrealistically dense stellar wind. Ghisellini et al. (2007b) showed that the optical/UV spectrum of the source is too bright for the X-ray and the optical to be parts of the same blackbody component. In response, Waxman et al. (2007) "fiercely argued"[8] that the shock breakout is anisotropic, and the different regions emit at different wavelengths, which helps to reconcile the theory with the observations. The prompt thermal X-rays are emitted by a compressed shell, while the optical radiation originates in the outer shells of the expanding star at a much larger radius. In their final reply, Ghisellini et al. (2007a) found the anisotropic expansion unconvincing. The simple energetics argument is dramatically inconsistent with the shock breakout model by Waxman et al. (2007). The isotropic optical thermal emission at $t \sim 10^3$ s requires a temperature of about $\sim 1 \times 10^6$ K, which corresponds to the total energy carried by a shock above 10^{51} erg, far in excess of any shock breakout model.

3.2. Jet Launched by a Magnetar or a Stellar Mass BH

A promising alternative explanation for GRB060218 is a jet launched by the central engine. A newborn central engine, a magnetar or a BH, results from a core collapse. A jet from this collapse pierces through the star and escapes. That is how a typical GRB operates and our source may just be on a low-luminosity end of the spectrum. A jet with a low Lorentz factor $\Gamma \sim 5$ and a wide opening angle $\theta \sim 0.3$ can produce

[8] (Ghisellini et al. 2007a, p. 2)

the emission, which peaks in the X-rays and exhibits no jet break (Toma et al. 2007). Such a jet may be powered over a long timescale by a magnetar. Central engine activity is a natural explanation for the afterglow (Soderberg et al. 2006; Fan et al. 2006). Dainotti et al. (2007) proposed a model of the interaction of an electron–positron fireshell and circumburst medium to explain the afterglow. Their best model constrains the density profile to $n \propto r^{-\beta}$, where $\beta = 1.0$–1.7 up to 10^{18} cm. The unusually bright prompt optical/UV emission can be explained by self-absorbed Comptonized synchrotron emission (Ghisellini et al. 2007b), while the blackbody X-rays result from photospheric jet emission (Ghisellini et al. 2007a). Bufano et al. (2012) argued that the central magnetar would spin down too rapidly and could not power the source over thousands of seconds while expending most of its energy in the expansion of the dense envelope. However, Quataert & Kasen (2012) proposed a model in application to Swift J1644+57 where a magnetar powers a GRB source over many days or even weeks.

A relativistic jet is a natural explanation for the source. However, if GRB060218 was a GRB, then it clearly was an unusual one. Long GRBs have large total energies $E_{\rm tot,iso} = 10^{52}$–$10^{54}$ erg (Nava et al. 2008), short durations $t_{90} = 2$–200 s (Butler et al. 2007), and higher Lorentz factors $\Gamma = 100$–1000 (Pe'er et al. 2007; Liang et al. 2010; Ghisellini 2012). The high Lorentz factor of a typical long GRB is the consequence of jet confinement by pressure from the star (Tchekhovskoy et al. 2010b). Bromberg et al. (2011) argued that the GRB population does not extend to the slow low-luminosity end. Thus, another origin of events such as GRB060218 is to be sought. Below we propose that the jet is launched by a tidal disruption. This model provides the explanations for the observed event duration, the spectrum, and the light curve.

4. TIDAL DISRUPTION MODEL

GRB060218 can be best modeled by a low-luminosity wide mildly relativistic outflow/jet. The tidal disruption of a WD by an IMBH produces such a jet. In this section, we discuss the expected temporal and spectral properties of such tidal disruptions, fit observations of GRB060218, and consider the accompanying supernova SN2006aj and its host galaxy. Extensive observations of the source pose multiple tests for any theory aimed at explaining it. The tidal disruption scenario passes all these tests.

4.1. Disruption Dynamics

4.1.1. Fallback Material and Disk Formation

A star is tidally disrupted when it comes sufficiently close to the BH. Let us define a tidal radius as

$$R_T = \left(\frac{2M_{\rm BH}}{m_{\rm WD}}\right)^{1/3} R_\star. \quad (2)$$

Only stars on orbits with a pericenter distance R_P smaller than about

$$R_P \lesssim R_T \quad (3)$$

can become disrupted (see Evans & Kochanek 1989 and references therein). The WD radius is (Nauenberg 1972)

$$R_\star = 8.5\times10^8\ {\rm cm}\left(\frac{m_{\rm WD}}{M_{\rm Ch}}\right)^{-1/3}\left[1-\left(\frac{m_{\rm WD}}{M_{\rm Ch}}\right)^{4/3}\right]^{1/2}, \quad (4)$$

where $M_{\rm Ch} = 1.44\,M_\odot$ is the Chandrasekhar mass. We calibrated the normalization to reproduce a typical observed WD radius (Nalezyty & Madej 2004) for one solar mass $m_{\rm WD} = 1\,M_\odot$. The tidal radius depends weakly on the BH mass, while the event horizon radius $R_{\rm g} = GM_{\rm BH}/c^2$ is proportional to the BH mass. Thus, SMBHs will swallow WDs without disruptions and only BHs with relatively small masses can disrupt WDs (Luminet & Pichon 1989a; Rosswog et al. 2009). The stars are swallowed if

$$R_P < f R_{\rm g}, \quad (5)$$

where $f \approx 8$ for a non-spinning BH, which captures massive geodesics with a specific angular momentum $\tilde{l} < 4R_{\rm g}c$ (Shapiro & Teukolsky 1986). The value of f can be much lower for spinning BHs (Kesden 2012). Combining Equations (2), (3), and (5), we find that only BHs with masses

$$M_{\rm BH} \lesssim \frac{\sqrt{2}c^3}{\sqrt{M_\star}}\left(\frac{R_\star}{fG}\right)^{3/2} \quad (6)$$

can tidally disrupt a star. The correspondent critical mass of a non-spinning BH to disrupt $0.8\,M_\odot$ WD is $3\times10^4\,M_\odot$. For a star on a parabolic orbit, about 50% of its material ends up being bound to the BH and about 50% remains unbound in a standard picture (Evans & Kochanek 1989). The fractions may change when the pericenter distance is close to the BH marginally bound orbit radius (several gravitational radii). Among models with different pericenter radii, BH spins, and orientations, Haas et al. (2012) found cases where almost all material is captured or almost all material remains unbound.

The bound material makes its way onto the BH. In classic theory, the fallback time is (Evans & Kochanek 1989)

$$t_{\rm fb} \sim \frac{R_P^3}{\sqrt{GM_{\rm BH}}R_\star^{3/2}} \quad (7)$$

and the fallback rate of debris is

$$\dot{M}_{\rm fb} = \frac{1}{3}\frac{M_\star}{t_{\rm fb}}\left(\frac{t_{\rm fb}}{t}\right)^{5/3}. \quad (8)$$

The fallback time $t_{\rm fb}$ can be anywhere from several hours to three minutes (Haas et al. 2012) for disruptions of WDs by IMBHs. The peak accretion rate is achieved at

$$t_{\rm peak} = \delta\frac{R_P^3}{\sqrt{GM_{\rm BH}}R_\star^{3/2}}, \quad (9)$$

where $\delta \approx 3.33$ for the adiabatic index $\Gamma_{\rm ad} = 5/3$ based on simulations by Evans & Kochanek (1989) and Laguna et al. (1993) for $\beta_T = R_T/R_P = 1$, while $\delta \approx 5.5$ for $\Gamma_{\rm ad} = 1.4$ (Lodato et al. 2009). Smaller values of the adiabatic index $\Gamma_{\rm ad} < 5/3$ are more appropriate for heavy WDs. The corresponding peak fallback rate is

$$\dot{M}_{\rm peak} \approx 0.05 m_{\rm WD}\frac{\sqrt{GM_{\rm BH}}R_\star^{3/2}}{R_P^3} \quad (10)$$

for $\Gamma_{\rm ad} = 1.4$. The fallback rate rises from zero, when the most bound debris just reaches the BH, up to the maximum value $\dot{M}_{\rm peak}$ at $t_{\rm peak}$ and then decreases according to $t^{-5/3}$ law.

The fallback matter forms an accretion disk at a circularization radius $R_{\rm circ} = \eta R_P$, where $\eta = 2$ according to the conservation of angular momentum. The disk exists as a radiatively

inefficient accretion flow (RIAF) since the material density is very high and the photons cannot escape (Abramowicz et al. 1988). The fallback rate determines the accretion rate during the early evolution of the system. After the disk is formed, it starts to evolve on a slow viscous timescale for $R_{\rm circ}$ radius (Cannizzo et al. 1990). Such evolution changes the temporal slope of the accretion rate to $t^{-4/3}$ for adiabatic RIAFs (Cannizzo et al. 2011). RIAFs with an outward energy flux may unbind the material in the outer disk (Narayan et al. 2001; Metzger 2012). Then only a small percentage of the material reaches the BH. However, inner disk regions with a radius less than $\sim 20\,R_{\rm g}$ evolve fast and are not influenced by relatively slow energy transport (Abramowicz et al. 2002).

As was recently shown by general relativistic magnetohydrodynamic simulations (Tchekhovskoy et al. 2011; McKinney et al. 2012), a poloidal magnetic field is necessary to launch a jet. The field strength for a strong jet can be estimated based on the equipartition argument. When the magnetic field energy density is comparable to the internal energy density of plasma as

$$\frac{B_{\rm BH}^2}{8\pi} \sim 0.1\frac{\dot{M}c}{4\pi R_{\rm g}^2} \sim 0.1 n_{\rm nuc} m_p c^2, \quad (11)$$

where $n_{\rm nuc}$ is the density of nucleons, and m_p is the proton mass. Then the magnetic field near the event horizon is

$$B_{\rm BH} \sim 1.3\times 10^{10}\left(\frac{\dot{M}}{10^3\,M_\odot\ {\rm yr}^{-1}}\right)^{1/2}\left(\frac{M_{\rm BH}}{10^4\,M_\odot}\right)^{-1}\ {\rm G}. \quad (12)$$

The magnetic field can reach 10^{15}–10^{16} G at the base of a GRB jet (Usov 1992; Wheeler et al. 2000; Uzdensky & MacFadyen 2007; Takiwaki et al. 2009). A powerful jet is launched after a WD disruption by an IMBH for $B_{\rm BH} \sim 10^{10}$ G. How can such a strong poloidal magnetic field be produced?

4.1.2. Generation of a Magnetic Field

The magnetic field lines get advected toward the BH event horizon with the fallback material. The magnetic field of a WD is typically within $B \lesssim 10^4$ G (Angel 1978; Putney 1999) with only a few examples of stronger fields. Since the WD radius is on the order of the BH gravitational radius, no field amplification is expected due to compression in the converging fallback flow. The BH may possess an accretion disk with a large magnetic field even before the disruption happens. When the accretion rate is close to the Eddington rate, the BH sustains the so-called Eddington magnetic field (Rees 1984; Daly 2011)

$$B_{\rm Edd} = 6\times 10^6\left(\frac{M_{\rm BH}}{10^4\,M_\odot}\right)^{-1/2}\ {\rm G}. \quad (13)$$

A somewhat larger magnetic field can be accumulated on a BH by infalling debris, which drags the pre-existing magnetic flux toward the event horizon. Such magnetic field generation is a promising mechanism for the source Swift J1644+57 (Tchekhovskoy et al. 2013). However, the required B-field amplification factor of 10^3 for the tidal disruption of a WD might not be attained by inward dragging of the pre-existing magnetic flux.

In situ amplification of the initial seed magnetic field into the equipartition poloidal magnetic field is needed to sustain a powerful jet. Magnetorotational instability (MRI; Balbus & Hawley 1991, 1998) can increase the turbulent magnetic field strength with an e-folding time of three orbital periods (Stone et al. 1996). Growth by a factor of 10^3 can be achieved over $\sim$25 local orbits. The orbital period is (Bardeen et al. 1972; Shapiro & Teukolsky 1986)

$$t_{\rm orb} = \frac{2\pi R_{\rm g}}{c}\left[\left(\frac{R_{\rm ISCO}}{R_{\rm g}}\right)^{3/2} + a^\star\right] \approx 2.5\left(\frac{M_{\rm BH}}{10^4\,M_\odot}\right)\ {\rm s}. \quad (14)$$

at the innermost stable circular orbit (ISCO) for a dimensionless spin $a^\star = 0.6$. In sum, a $10^4\,M_\odot$ BH can amplify the random magnetic field 10^3 times in as little as 60 s.

MRI turbulence produces a random B field, while a regular poloidal magnetic field is needed to launch a jet. Magnetic field generation in a turbulent medium should occur via dynamo action (Brandenburg & Subramanian 2005), which operates on a viscous timescale determined by the radial velocity v_r (Davis et al. 2010; O'Neill et al. 2011). A geometrically thick accretion flow with an effective dimensionless viscosity $\alpha = 0.1$–0.3 (King et al. 2007) has a radial velocity $v_r \lesssim \alpha v_K$, where v_K is the Keplerian velocity. The viscous timescale at the ISCO can be as short as 15 s for a $10^4\,M_\odot$ BH. Substantial generation of the regular poloidal field component is expected over $\gtrsim$10 viscous timescales or $\gtrsim$150 s. The failure of previous attempts to generate a magnetic field via dynamo action might arise from the low resolution in those simulations (J. McKinney 2012, private communication). In sum, it might be possible to generate a substantial poloidal magnetic field before the estimated accretion rate peak time.

4.1.3. Jet Launching

A jet is a relativistic outflow of material from near the BH. A spinning BH surrounded by accreting magnetized gas is expected to launch a jet (Blandford & Znajek 1977). We can estimate the jet power via a Blandford–Znajek formula. When the magnetic field energy density reaches equipartition with the matter energy density close to the BH, then the Blandford–Znajek jet power is approximately (McKinney 2005; Tchekhovskoy et al. 2010a)

$$L_{\rm kin} \sim P_0 a^{\star 2}\dot{M}c^2. \quad (15)$$

While simulations with the maximum magnetic flux were capable of reaching $P_0 \sim 1$ (Tchekhovskoy et al. 2011; McKinney et al. 2012), more traditional values observed in simulations with the weak initial field are $P_0 = 0.01$–0.1 (McKinney & Blandford 2009; Penna et al. 2010). The tidal disruption of a WD by an IMBH has a typical maximum accretion rate of $\dot{M}_{\rm peak} \sim 10^4\,M_\odot\ {\rm yr}^{-1}$ according to formula (10). This corresponds to a jet power $L_{\rm kin} \sim 0.01\dot{M}c^2 = 5\times 10^{48}\ {\rm erg\ s}^{-1}$. Since there is no theoretical understanding of whether or not dynamo action would quickly generate a poloidal magnetic field, the kinetic power estimated by Equation (15) is an upper limit. The actual jet power may be substantially lower.

The kinematics of the jet are characterized by the bulk Lorentz factor Γ. GRB jets have very high $\Gamma = 100$–1000 likely because of confinement by the surrounding star (Tchekhovskoy et al. 2010b). In turn, jets in active galactic nucleus (AGN) are not strongly confined by ambient gas. Their Γ factors are about $\Gamma \sim 10$ (Jorstad et al. 2005; Pushkarev et al. 2009). Similarly, jets from low-mass X-ray binaries have bulk Lorentz factors of about $\Gamma \sim 10$ (Miller-Jones et al. 2006). The tidal disruption debris is expected to scatter in the radius, cool, and provide little pressure support for the jet regardless of the direction in

Table 1
Time-resolved Spectroscopy with a Broken Power-law Model

Number	Time Period t (s)	Break Energy $E_{\rm break}$ (keV)	High-energy Slope Γ_2	Absorbed Flux $F_{\rm abs}$ (10^{-9} erg s^{-1} cm^{-2})	Unabsorbed Source Flux $F_{\rm unabs}$ (10^{-9} erg s^{-1} cm^{-2})
1	164–478	0.795	1.226	4.753	5.234
2	478–691	0.740	1.171	7.411	8.148
3	691–875	0.820	1.234	8.242	9.064
4	875–1049	0.746	1.290	8.572	9.575
5	1049–1226	0.813	1.419	7.595	8.575
6	1226–1414	0.800	1.519	6.780	7.795
7	1414–1620	0.761	1.650	5.583	6.631
8	1620–1854	0.749	1.816	4.421	5.467
9	1854–2119	0.678	1.962	3.621	4.783
10	2119–2404	0.712	2.190	2.940	4.110
11	2404–2756	0.656	2.332	2.265	3.457

Notes. The parameters of the XSPEC *bknpower* model are shown. The low-energy slope of the count spectrum is fixed at $\Gamma_1 = -1$, which corresponds to the Raleigh–Jeans tail of the blackbody emission with $F_\nu \propto \nu^2$. The host galaxy hydrogen column density $N_{\rm H} = 0.750 \times 10^{22}$ cm^{-2} with a metallicity 0.07 of solar (Wiersema et al. 2007) provides the best joint fit to all time slices with $\chi^2 = 5463.0$ for 4836 dof. The galactic column is fixed at $N_{\rm H} = 9.4 \times 10^{20}$ cm^{-2} following Campana et al. (2006).

which the debris is scattered. Therefore, a tidal disruption jet is expected to have $\Gamma \sim 10$. A low Lorentz factor $\Gamma \sim 10$ is in fact suggested for a Swift J1644+57 tidal disruption event (Metzger et al. 2012; Liu et al. 2012).

4.2. Prompt X-Ray Emission

Prompt X-ray emission from a slow jet is expected to have a Comptonized blackbody spectrum produced near the jet photosphere. We perform time-resolved spectroscopy of *Swift* XRT observations of the source and fit the spectrum with a Comptonized blackbody model. We follow Butler (2007) and cut the full XRT window mode observations into 11 time slices with about 16,000 photons in each. We run *xrtpipeline*, select the time slices with *xselect*, take the appropriate response matrix files from the calibration database (CALDB version 11) as indicated by the *xrtmkarf* routine within the pipeline, and use the ancillary response files generated by *xrtpipeline*. We run *grppha* to group nearby bins to have at least 20 photons per bin and perform the minimization of least squares. We model the spectrum in XSPEC v12.7 (Arnaud 1996) with a broken power law *bknpower* and with the blackbody spectrum Comptonized by thermal electrons as a part of a *compPS* model (Poutanen & Svensson 1996). We favor the exact *compPS* model over approximate prescriptions for thermal Comptonization of the blackbody spectrum such as *compBB* (Nishimura et al. 1986) and *compTT* (Titarchuk 1994). We compute the model flux in the 0.05–10 keV band to capture very soft thermal X-rays. Unlike Butler (2007) and Campana et al. (2006), we consider the host galaxy to be a low-metallicity absorber with $Z = 0.07\ Z_\odot$ (Wiersema et al. 2007) while, following Campana et al. (2006), we fix the Galactic column at $N_{\rm H} = 9.4 \times 10^{20}$ cm^{-2} with the solar metallicity. We ignore any potential changes of the hydrogen absorption column with time. We search for a joint best fit to all time slices with a single host galaxy $N_{\rm H}$.

The results of spectral fitting are presented in Table 1 for the broken power-law fits. A substantial degeneracy exists between the soft power-law slope in a *bknpower* model and the host $N_{\rm H}$. We fix the soft photon index at $\Gamma_1 = -1$, which is representative of the Rayleigh–Jeans tail $F_\nu \propto \nu^2$ of the blackbody. The host galaxy hydrogen column $N_{\rm H} = 0.750 \times 10^{22}$ cm^{-2} provides the best joint fit to all time slices with $\chi^2 = 5463.0$ for 4836 degrees of freedom (dof). The break energy is 0.7–0.8 keV and depends weakly on the total flux. Since the emission becomes substantially softer with time, the absorbed flux constitutes a much smaller fraction of the unabsorbed flux at late times. This masks the true temporal evolution of the source flux.

The results of spectral fitting are presented in Table 2 for the blackbody spectrum Comptonized by thermal electrons as computed within a *compPS* XSPEC model. The optical depth of Compton scattering is fixed at $\tau_\sigma = 1$ for scattering at the photosphere. The host galaxy hydrogen column $N_{\rm H} = 1.090 \times 10^{22}$ cm^{-2} provides the best joint fit to all time slices with $\chi^2 = 5358.9$ for 4836 dof. The fit is slightly better for this model compared to the *bknpower* model. Our fit has a higher blackbody flux fraction at the peak (40%) compared to a ∼15% fraction in a fit by Campana et al. (2006) who employed the solar metallicity of the absorber and used a sum of the power law and the blackbody. Table 2 also summarizes application of the fireball model (Pe'er et al. 2007) to the blackbody emission component. We can estimate the bulk Lorentz factor of the flow Γ and the jet base radius knowing the temperature $T_{\rm BB}$, the observed isotropic flux $F_{\rm BB}$, the distance to the source, and assuming a fiducial ratio $Y = 10$ of the total fireball energy to the energy emitted in X-rays/γ-rays. The jet parameters obtained are surprisingly consistent between different time slices, which might indicate that the fireball model captures the physics of the event. The bulk Lorentz factor of $\Gamma \approx 2.7 Y_{10}^{1/4}$ corresponds to a mildly relativistic jet, while the jet base radius is $R_0 = (1.0\text{–}1.7) \times 10^{10} Y_{10}^{-3/2}$ cm. The model is self-consistent for a wide range of Y as the saturation radius $R_s = \Gamma R_0$ lies well within the photosphere with a radius $R_{\rm ph} \sim 5 \times 10^{12}$ cm. The jet-launching region should be located at several BH gravitational radii. Assuming that the jet base radius is at $R_0 = 5\ R_{\rm g}$, we find the BH mass $M_{\rm BH} = (1.3\text{–}2.3) \times 10^4\ Y_{10}^{-3/2}\ M_\odot$, which places the BH into the intermediate-mass category. Pe'er et al. (2007) argue that the ratio of energies is $Y_{10} \lesssim 1$.

The reduced chi-squared $\chi^2/{\rm dof} = 1.138$ for the joint *bknpower* fit and $\chi^2/{\rm dof} = 1.115$ for the joint *compPS* fit are quite low despite good photon statistics. Even better fits down to $\chi^2/{\rm dof} = 1.0$ can be achieved when the host galaxy hydrogen column density is allowed to vary between the time slices as in Butler (2007). However, we do not see a physical reason for $N_{\rm H}$ to vary on a timescale of 10^3 s, which corresponds to 3×10^{13} cm in distance, while the characteristic star formation

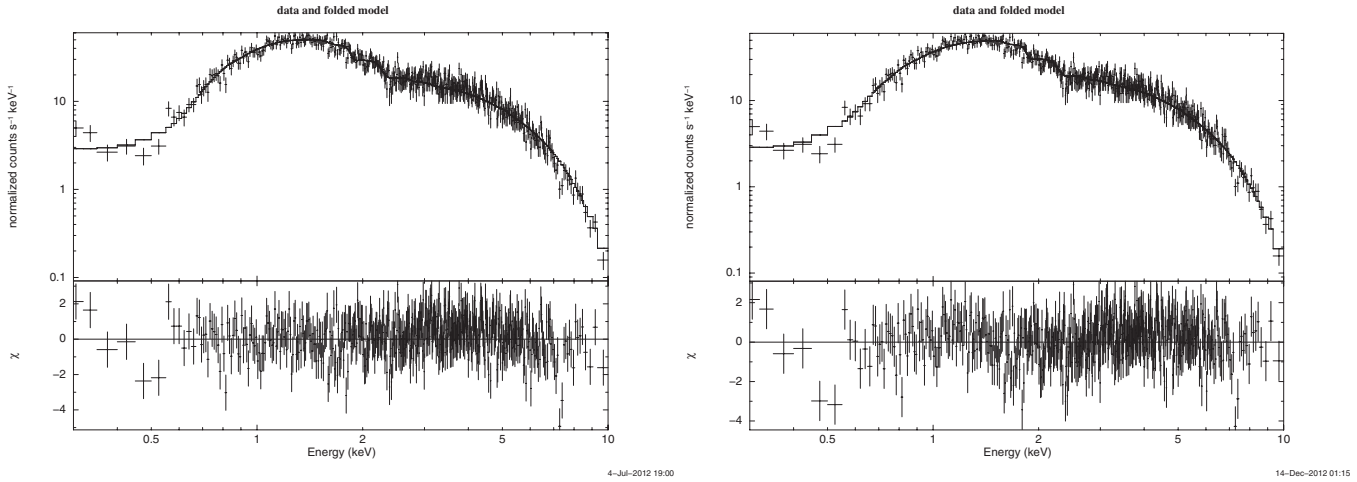

Figure 1. Parts of XSPEC spectral fits and normalized residuals for the 4th time slice. This time slice corresponds to the highest soft X-ray flux. The left panel shows the results for the *bknpower* model and the right panel shows the results for the blackbody spectrum Comptonized by thermal electrons within the *compPS* model. The model parameters can be found in Tables 1 and 2.

Table 2
Time-resolved Spectroscopy with a Blackbody Spectrum Comptonized by Thermal Electrons

Number	Time Period t (s)	Photon Temperature T_0 (keV)	Electron Temperature T_e (keV)	Absorbed Flux $F_{\rm abs}$ (10^{-9} erg s^{-1} cm^{-2})	Unabsorbed Source Flux $F_{\rm unabs}$ (10^{-9} erg s^{-1} cm^{-2})	Blackbody Source Flux $F_{\rm BB}$ (10^{-9} erg s^{-1} cm^{-2})	Lorentz Factor $\times Y_{10}^{1/4}, \Gamma$	Jet Base Radius $\times Y_{10}^{-3/2}$, R_0 (10^{10} cm)
1	164–478	0.1039	262.3	4.586	6.61	2.630	2.667	0.906
2	478–691	0.1052	297.6	7.159	10.17	4.033	2.832	1.091
3	691–875	0.0994	258.8	7.965	11.49	4.465	2.803	1.245
4	875–1049	0.1058	230.2	8.353	12.29	5.020	2.898	1.257
5	1049–1226	0.0967	176.6	7.424	11.52	4.763	2.744	1.493
6	1226–1414	0.1008	145.8	6.636	10.84	4.848	2.753	1.560
7	1414–1620	0.1119	119.5	5.517	9.56	4.784	2.816	1.487
8	1620–1854	0.1116	93.1	4.369	8.43	4.686	2.732	1.733
9	1854–2119	0.1324	80.9	3.614	7.16	4.412	2.879	1.393
10	2119–2404	0.1489	65.9	2.970	6.25	4.284	2.961	1.275
11	2404–2756	0.1421	55.3	2.268	5.41	3.963	2.818	1.485

Notes. The parameters of the blackbody spectrum Comptonized by thermal electrons within a *compPS* model are shown. The optical depth is fixed at $\tau_\sigma = 1$, which corresponds to Compton scattering at the photosphere. We find the host galaxy hydrogen column density $N_{\rm H} = 1.090 \times 10^{22}$ cm^{-2} in a self-consistent joint fit over all time slices with $\chi^2 = 5358.9$ for 4836 dof. The Galactic column is fixed at $N_{\rm H} = 9.4 \times 10^{20}$ cm^{-2} with solar metallicity following Campana et al. (2006). The quantity Y_{10} is the ratio of the total fireball energy to the energy emitted in X-rays in units of 10. The last two columns are computed for $Y_{10} = 1$ or $Y = 10$ within the thermal fireball emission model described in Pe'er et al. (2007). The jet base radius $R_0 \sim 10^{10}$ cm corresponds to the BH mass $M_{\rm BH} \sim 10^4\, M_\odot$ assuming the jet is launched within several $R_{\rm g}$ from the center.

size of the host galaxy is $R_{80} = 0.55$ kpc $= 10^{21}$ cm (Svensson et al. 2010). To test for potential discrepancies between the fits and the observations, in Figure 1 we depict the parts of the fits and the normalized residuals for the 4th time slice characterized by the highest soft X-ray flux. The left panel shows the results for the *bknpower* model, while the right panel shows the results for a blackbody spectrum Comptonized by thermal electrons. The residuals do not systematically deviate from zero except slightly at very low energies or for certain absorption features. At low energies, the *Swift* XRT response might be uncertain or the line physics might alter the spectrum. The most prominent absorption feature is around 7.3 keV.

4.3. Prompt Optical/UV Emission

The prompt optical/UV emission observed by the UVOT instrument on board the *Swift* satellite was a matter of major disagreement between the former theoretical models. The same blackbody component cannot produce both the optical and the X-ray emission (Ghisellini et al. 2007b), which is consistent with the physical picture within the tidal disruption scenario. For an estimate we take the magnetic field in the photosphere to be in equipartition with the jet kinetic energy. Then the Poynting energy flux is about $Y/2 \sim 5$ times larger than the total X-ray radiation flux. Hence, the magnetic field in the photosphere has a strength

$$B_{\rm ph} \sim 10^5 \text{ G}. \quad (16)$$

The *compPS* fit to the prompt X-ray spectrum shows that non-thermal particles with energies ~200 keV exist in the photosphere. The fact that the emission continues to hard X-rays in the BAT band reveals the existence of much more energetic particles with $\gamma \sim$ 10–100, which readily emit synchrotron emission in the optical band. Synchrotron emission by an electron with a random Lorentz factor $\gamma \sim 30$ peaks at 300 nm for a 10^5 G magnetic field. Since the effective synchrotron cross-section is much higher than the Thompson scattering cross-section, the optical photosphere is far above the X-ray photosphere. In fact, the very large jet particle density makes the optical photosphere coincide with the front of the jet propagating with a bulk Lorentz factor $\Gamma \sim 3$ into the surrounding medium. The jet front can propagate up to $R_{\rm front} = t_{\rm obs}\Gamma^2 c$, where $t_{\rm obs}$ is the time since

BAT trigger. Continuous energy dissipation and particle acceleration at the front ensures there are enough energetic electrons to produce optical/UV synchrotron emission. Note that the interactions with the interstellar medium at early times, which lead to a forward shock, may contribute less to the emission. A low magnetic field at the jet front

$$B_{\rm front} \sim 10^3 \ {\rm G} \quad (17)$$

at $t_{\rm obs} = 3 \times 10^3$ s is compensated by higher Lorentz factors $\gamma \sim 300$ of the electrons producing the optical/UV emission.

The idea of jet front emission explains the steep $F_\nu \propto \nu^2$ spectrum and the achromatic flux growth at different UVOT frequencies up to $\sim 3 \times 10^4$ s. The jet front is transparent to hard UV and X-ray photons. Since the particles are subject to rapid cooling, the spectrum of re-accelerated particles may substantially deviate from a power law and resemble a very hot Maxwellian. Thus the resultant self-absorbed spectrum could be the Rayleigh–Jeans part of the blackbody $F_\nu \propto \nu^2$ as opposed to the absorbed synchrotron $F_\nu \propto \nu^{5/2}$ spectrum (Rybicki & Lightman 1979). The observed temperature of the optical/UV radiation is about 10^6 K (Ghisellini et al. 2007a), which violates the energetics of the source in a non-relativistic emission model with total emitted energy $E_{\rm BB} \gtrsim 10^{51}$ erg. In turn, the relativistic jet front emission does not violate the source energetics. Relativistic Doppler boosting with $\Gamma \sim 3$ reduces the emission temperature down to $\lesssim 3 \times 10^5$ K, which readily leads to $E_{\rm BB} \lesssim 10^{50}$ erg. The inferred large optical emission radius 10^{14}–10^{15} cm at 3×10^3 s is consistent with $R_{\rm front}$ for the mildly relativistic expanding shell. A more detailed jet model for optical/UV emission by Ghisellini et al. (2007b) is similarly consistent with the source energetics.

4.4. Temporal Analysis

The spectral modeling allows for proper determination of fluxes at different times to study the temporal behavior of the source. Figure 2 shows the absorbed and unabsorbed source fluxes as functions of time. The soft X-ray flux peaks at around 800 s following triggering of *Swift* BAT. We fit the light curve with the scaled accretion rate dependence on time $\dot{M}(t)$ for a tidal disruption of a MS star by a SMBH. Such a dependence for $\beta_T = 1$ was taken from Laguna et al. (1993). The best fit corresponds to a time delay of $\Delta t = 1810$ s between the tidal disruption and triggering of *Swift* BAT. The peak at $t_{\rm peak} \approx 2600$ s corresponds, for example, to the tidal disruption of a $m_{\rm WD} = 0.75\,M_\odot$ WD by a $1 \times 10^4\,M_\odot$ IMBH (or a $m_{\rm WD} = 0.86\,M_\odot$ WD by a $2 \times 10^4\,M_\odot$ IMBH) at $\beta_T = 1$. The tidal radius in this case is $16R_{\rm g}$ (or $8R_{\rm g}$). A deeper encounter with $\beta_T > 1$ may be needed to initiate nuclear burning for an accompanying supernova, but the dependence of critical β_T, when effective nuclear burning starts, on the WD and BH masses is not known at present. The encounter in question may indeed have a very small pericenter distance with $\beta_T \gg 1$ and not violate the peak time constraint. The dependence of peak times on β_T is found to be very weak in numerical simulations (De Colle et al. 2012; Guillochon & Ramirez-Ruiz 2013) as well as in theoretical modeling (Stone et al. 2012). The accretion rate curve $\dot{M}(t)$ provides a good fit to the unabsorbed source flux. However, such a fitting procedure is prone to multiple caveats. First, the accretion disk around the BH takes a finite amount of time $t_{\rm magn} \sim 100 t_{\rm orb} \sim 250$ s to generate a strong poloidal magnetic field. Despite the magnetic field generation time being much less than the characteristic dynamical time

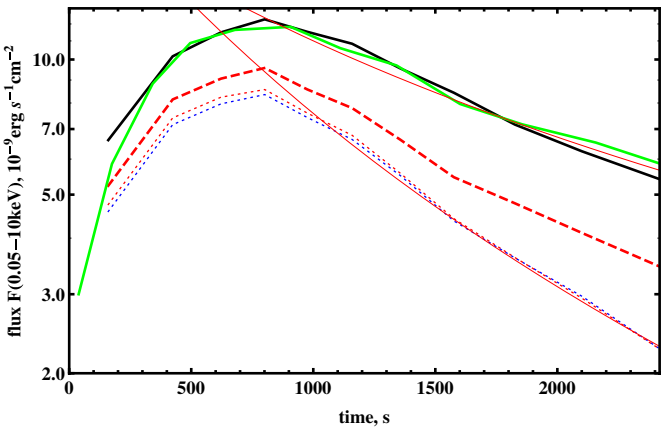

Figure 2. Soft X-ray light curve of GRB060218 fitted with the accretion rate temporal evolution $\dot{M}(t)$. Shown are the unabsorbed source light curve for the *compPS* model (dark black solid line) and for the *bknpower* model (red dashed line), the observed absorbed light curve for the *compPS* model (lower blue dotted line) and for the *bknpower* model (upper red dotted line), and the scaled fallback accretion rate based on Laguna et al. (1993; green solid line). The scaled accretion rate is offset by $\Delta t = 1810$ s, which is the time the most bound debris takes to reach the BH. Two thin red lines $(t + \Delta t)^{-3}$ and $(t + \Delta t)^{-5/3}$ are shown to emphasize the asymptotic behavior of the absorbed flux and the unabsorbed flux, respectively. While the observed flux decays as $F \propto t^{-3}$, the unabsorbed flux exhibits $F \propto t^{-5/3}$ late-time behavior in agreement with the tidal disruption scenario.

(A color version of this figure is available in the online journal.)

$t_{\rm magn} \ll t_{\rm dyn} \sim 1000$ s, a precise fit is not expected. Second, the transition from the accretion power $\dot{M}c^2$ to the emission power in a certain band is not trivial. Jets are expected to be radiatively efficient (Pe'er et al. 2007), and most of the emission, especially at late times, falls into the 0.05–10 keV band. The soft X-ray luminosity is expected to approximately follow the accretion power only if the jet's kinetic power is a constant fraction of the accretion power. Finally, general relativistic effects are not included in these estimates. Haas et al. (2012) emphasized that ultra-close encounters with small $R_P \sim$ several $\times\, R_{\rm g}$ may lead to a non-trivial temporal behavior of $\dot{M}$.

The estimated large BH mass and the small Lorentz factor may lead to a smooth light curve. The light curves of typical GRBs are highly variable, which is attributed to fast variations near small BHs with masses $M_{\rm BH} \sim 10\,M_\odot$ when BHs launch shocks at different speeds. The variation timescale is correspondingly longer for BHs with much larger masses $M_{\rm BH} \sim 10^4\,M_\odot$. These variations amplify when shocks moving at different high Lorentz factors collide. The energy release and the radiated energy are relatively small when shocks with small Γ's collide. Lastly, collisions between slow-moving shocks are likely to happen inside the photosphere so any variations are smoothed. Thus, a slow-moving jet of GRB060218 is expected to vary on a very long timescale and the variations are expected to be small. The object should exhibit a smooth light curve. In Figure 3, we present the log-smoothed periodograms $I(T)$ (Papadakis & Lawrence 1993) of GRB060218 and other light curves. The dark (blue) rising curve is the periodogram of GRB060218 prompt X-rays. The dark (red) constant curves are the periodograms of 20 white noise implementations with the same mean count rates and total counts as GRB060218. The light (green) curves represent the selection from the online *Swift* catalog of 16 GRBs whose peak photon count rates are the closest to the peak count rate of 148 counts s^{-1} of GRB060218. The white noise implementations are flat, as expected, while our

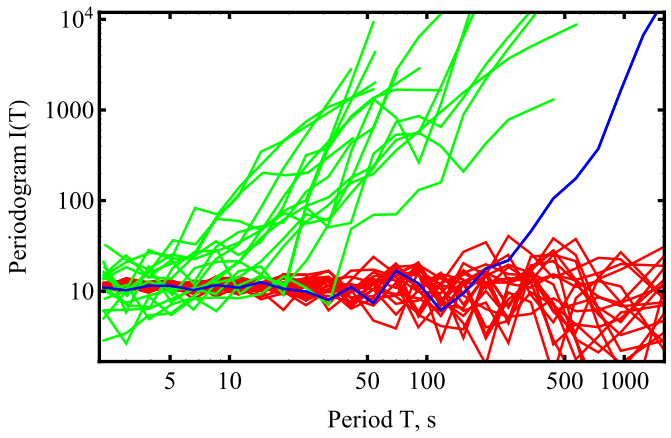

Figure 3. Log-smoothed periodograms $I(T)$ (Papadakis & Lawrence 1993) of the light curves binned to 1 s. The flat red curves depict simulated white noise, GRB060218 is shown by a dark/blue curve, while 16 other GRBs are shown by light/green curves. The white noise has the same mean count rate and total counts as GRB060218. The other GRBs are selected to have a peak count rate between 142 counts s^{-1} and 166 counts s^{-1}, while the peak count rate is 148 counts s^{-1} for GRB060218. The break time t_b, at which the periodogram starts deviating substantially from the noise, corresponds to a characteristic system timescale. The break time for our event is $t_b \sim 300$ s, which is consistent with the emission rise timescale in tidal disruption. Other GRBs have substantially lower break times $t_b = 5$–40 s, and the distribution of t_b does not continue to 300 s. This indicates a different origin of GRB060218. Log-smoothing is performed to 0.11 dex.

(A color version of this figure is available in the online journal.)

candidate tidal disruption source rises above the noise at a very long break time of about $t_b = 300$ s. The other 16 GRBs show much smaller break times of 5–40 s. For some of the sources the break time coincides with the characteristic flux decay time, while most sources exhibit variability on a shorter timescale. As predicted, the light curve of GRB060218 is smooth and shows no variability faster than the emission rise timescale. This strengthens the case for the source being a slow dense jet from an IMBH.

4.5. Steep Decay Phase and Afterglow

The *Swift* satellite was unable to observe the source from 2780 s through 5900 s from triggering of the BAT. The observed X-ray flux at 5900 s is very low, which is seemingly inconsistent with $t^{-5/3}$ behavior of the accretion rate. However, the blackbody source flux may still be large, while the observed flux may be a factor of 40 lower due to the action of absorption and incomplete overlap with the XRT band. The XRT instrument observes mostly Comptonized photons with an effective energy range 0.3–10 keV. The energy of the Comptonizing electrons decreases with time during the prompt phase, which translates into a ratio of unabsorbed to absorbed fluxes rising from 1.4 to 2.4 by the 11th time slice (see Table 2). The ratio of fluxes keeps dropping until 10^4 s in the steep decline phase. After that a much shallower decline $F \propto t^{-1.2}$ follows (Campana et al. 2006) with a spectrum consistent with a power-law $F_\nu \propto \nu^{-2.2}$ (Soderberg et al. 2006). While the temporal decay of this late phase is consistent with the afterglow, the spectrum is substantially softer than the typical afterglow spectrum emitted by the external shock (Toma et al. 2007). The softer spectrum and the long afterglow may be explained by the late activity of the source (Soderberg et al. 2006). This is an especially viable idea since the kinetic luminosity of the jet is expected to stay high for a long period of time following a tidal disruption.

We model the steep decay spectrum within a time interval $t = (5950, 7070)$ s with a combination of a blackbody component Comptonized by thermal electrons and power-law emission from the external shock. We fix the absorption at the level determined with *compPS* fitting of the prompt X-ray emission. The fit allows for a large range of power-law slopes without a significant change in χ^2. We fix the power-law slope at $\Gamma_{\rm pl} = 2$ ($F_\nu \propto \nu^{-1}$), which corresponds to the afterglow of a typical GRB (Soderberg et al. 2006). The absorbed combination of the *compPS* and *powerlaw* models leads to $\chi^2 = 43.1$ for 36 dof. As suggested by Butler (2007), the spectrum contains lines that become prominent at late times. Lines are the natural outcome of the atomic processes in warm absorbing/emitting baryonic jet material. The baryonic jet material consists of WD debris rich in oxygen and carbon and practically devoid of hydrogen. The absorption by cooled down jet exhaust may become strong at late times. We model such absorption with a blueshifted *zvphabs* model where we set the abundance of a single chemical element at 1000 and the abundances of the other elements at 0. The model with a pure oxygen cold absorber converges to a blueshift $z = -0.422$, which corresponds to the bulk Lorentz factor $\Gamma = 1.73$ consistently with the fits to the prompt spectrum. The fit with $\chi^2 = 37.3$ for 36 dof and the normalized residuals are depicted in Figure 4. The fit can be marginally improved with the addition of iron elements. We do not present such modeling here for simplicity. The addition of carbon with abundance of 30% of oxygen abundance does not change the fit. The best-fitting oxygen column density $N_{\rm O} = 1 \times 10^{18}$ cm^{-2} can be readily provided by the cooling jet material. A very soft blackbody has a temperature $T = 0.052$ keV. The best-fitting flux is $F_{\rm unabs}(0.05\text{–}10\,{\rm keV}) = 1.8 \times 10^{-9}$ erg s^{-1} cm^{-2}, which directly traces the $t^{-5/3}$ decay law from the time of the peak flux, while the observed absorbed flux $F_{\rm abs} = 4.0 \times 10^{-11}$ erg s^{-1} cm^{-2} is 40 times lower. The absorbed power-law contribution to the total source flux is $F_{\rm abs,pl} = 2.5 \times 10^{-11}$ erg s^{-1} cm^{-2}, which is consistent with the emission at later times being dominated by a power law. The application of the photospheric emission model (Pe'er et al. 2007) to determine the Lorentz factor and the jet base radius gives $\Gamma = 1.45 Y_{10}^{1/4}$ and $R_0 = 1.1 \times 10^{11} Y^{-3/2}$ cm, respectively. A larger ratio of total to radiated energy $Y = 4 \times Y_{\rm prompt}$ makes the numbers consistent with the results from the prompt phase. Since the blackbody is too soft to be directly observed, there is a substantial degeneracy between its temperature and normalization, which leads to the unabsorbed flux being uncertain by a factor of three. Taking this uncertainty into account, the unabsorbed flux $F_{\rm unabs}$ is consistent with the $t^{-5/3}$ law even for larger Y. We might not be able to compute a more self-consistent physical model of the steep decay phase unless we incorporate the atomic physics of warm emitters/absorbers, which is beyond the scope of the present paper.

The accretion rate law switches from $t^{-5/3}$ fallback-dominated behavior to $t^{-4/3}$ behavior determined by disk viscous spreading (Kumar et al. 2008; Cannizzo & Gehrels 2009; Cannizzo et al. 2011). The time of this transition as estimated by Cannizzo et al. (2011) is

$$t_{x1} = 1.25 \times 10^{10}\ {\rm s} \left(\frac{M_\star}{M_\odot}\right)^{-3/2} \left(\frac{R_\star}{R_\odot}\right)^{3/2} \times \left(\frac{M_{\rm BH}}{10^7\, M_\odot}\right) \left(\frac{\alpha}{0.1}\right) \left(\frac{\eta}{2\beta_T}\right)^{9/2}, \quad (18)$$

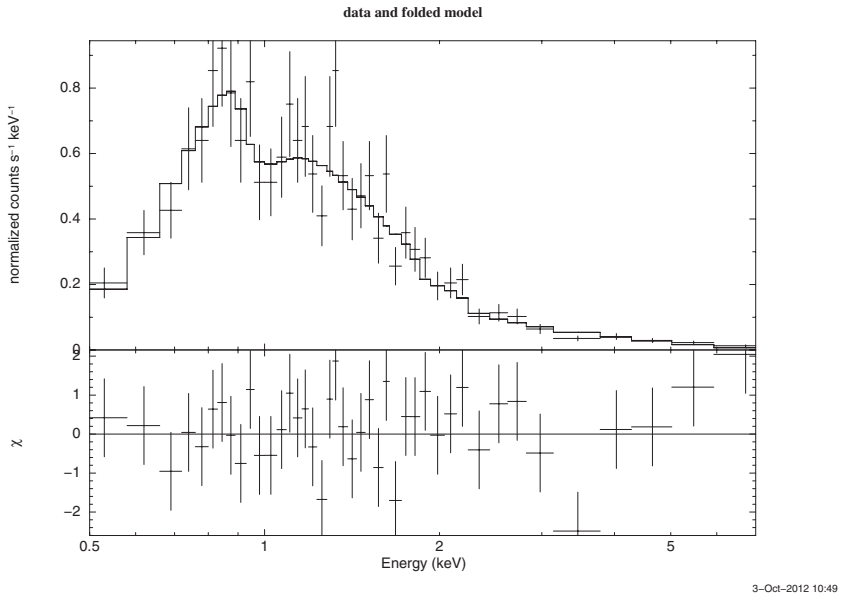

Figure 4. Best fit to the spectrum at the late times $t = (5950, 7070)$ s with $\chi^2 = 37.3$ for 36 dof. The model consists of the blackbody emission Comptonized by thermal electrons absorbed by blueshifted oxygen and a power law with a fixed slope $\Gamma_{\rm pl} = 2$ ($F_\nu \propto \nu^{-1}$). The sum of these two components is absorbed by the galactic $N_{\rm H} = 9.4 \times 10^{20}$ cm^{-2} and $N_{\rm H} = 1.090 \times 10^{22}$ cm^{-2} of the host galaxy with their respectively metallicities all fixed from the early-time modeling. The blueshift $z = -0.422$ corresponds to the bulk Lorentz factor $\Gamma = 1.73$. The best-fitting cold oxygen column density is $N_{\rm O} = 1 \times 10^{18}$ cm^{-2}, which can be readily provided by cooling jet exhaust. The blueshifted oxygen manifests as an absorption feature around 1 keV. The unabsorbed source flux in $F_{\rm unabs}(0.05\text{–}10\ {\rm keV}) = 1.8 \times 10^{-9}$ erg s^{-1} cm^{-2}, which coincides with the extrapolation based on $t^{-5/3}$ law, while the heavily absorbed observed flux is $F_{\rm abs} = 4.0 \times 10^{-11}$ erg s^{-1} cm^{-2}.

where as before $\eta = 2$ is the ratio of initial disk radius to pericenter radius. The implicit assumption in Cannizzo et al. (2011) is that all debris forms a disk, which then viscously spreads. However, the viscous time at the disk outer boundary, or the accretion time, is initially much lower than the time since disruption (Ulmer 1999; Kumar et al. 2008; Strubbe & Quataert 2009), and the debris falls onto the BH as opposed to accumulating in a disk. Let us take a proper account of the fast accretion timescale and perform a refined estimate of the transition time t_x. We make a one-zone approximation where most of the mass and angular momentum of the disk are located near a single radius $R_{\rm disk}$. The disk radius increases with time from the initial $R_{\rm disk} = 2R_P$. The disk mass $M_{\rm disk}$ also increases with time. Relatively little angular momentum transfer happens between the disk and the BH. The angular momentum of debris

$$L_{\rm disk} = M_\star \sqrt{G M_{\rm BH} R_P/2} = {\rm const} \tag{19}$$

becomes the preserved angular momentum of the disk after most of the debris falls onto the BH. We took the debris mass to be $M_\star/2$. The disk angular momentum is expressed through the current mass and radius of the disk as

$$L_{\rm disk} = M_{\rm disk} \sqrt{G M_{\rm BH} R_{\rm disk}}. \tag{20}$$

The viscous time of the disk or the accretion time is

$$t_{\rm visc} = \frac{R_{\rm disk}^{3/2}}{\sqrt{\alpha G M_{\rm BH}}} \tag{21}$$

for disk thickness $H = R$. The infalling debris stays within the disk for only $t_{\rm visc}$, thus the disk mass is

$$M_{\rm disk} = \dot{M}_{\rm fb} t_{\rm visc}, \tag{22}$$

where the fallback rate $\dot{M}_{\rm fb}$ is given by formula (8). It can be seen from the above equations that $t_{\rm visc} \propto t^{5/4}$. While initially the viscous time is small $t_{\rm visc} < t$ as noted by Ulmer (1999) and Strubbe & Quataert (2009), equality is achieved later at the transition time t_x. Solving Equations (19)–(22) we find another estimate for the transition time

$$t_{x2} = \frac{2\sqrt{2\alpha G M_{\rm BH}} t_{\rm fb}^2}{27 R_P^{3/2}}, \tag{23}$$

where the fallback time $t_{\rm fb} \approx 2700$ s is inferred from the observed light curve. At late times $t > t_{x2}$ the viscous time becomes longer than the time since disruption. Then the fallback-dominated behavior gives way to spreading disk behavior, and the disk mass becomes larger than the mass of debris that has yet to fall back onto the disk.

Taking a WD with mass $0.86(0.75)\,M_\odot$ and radius $R_\star = 7.1(8.1) \times 10^8$ cm disrupted by a $2.0(1.0) \times 10^4\,M_\odot$ BH, we estimate the transition time to be $t_{x1} = 2.6(1.6) \times 10^4$ s and $t_{x2} = 5.6(3.0) \times 10^4$ s for $\beta_T = 1$. The estimated transition time t_x crudely agrees with observations. Shallow disk spreading behavior takes over around the transition to the afterglow phase. The temporal index of the power-law flux decay -1.2 ± 0.1 during the afterglow (Soderberg et al. 2006) is consistent with a -1.33 index of the mass accretion rate at late times. Despite the estimated transition time crudely agreeing with observations, our one-zone calculation may not offer an ultimate answer for t_x. A self-similar solution of disk spreading behavior by Lynden-Bell & Pringle (1974) shows a small fraction of mass carrying angular momentum to a large radius, while the bulk of the disk mass is concentrated at a smaller distance from the central object serving as a reservoir for the infalling gas. Accordingly, a refined transition time estimate may show a longer t_x. Another important effect is cooling of the outer disk, which leads to its collapse onto an equatorial plane accompanied by a dramatic increases of the viscous time. A detailed computation is beyond the scope of the present paper, so we leave this topic to future research.

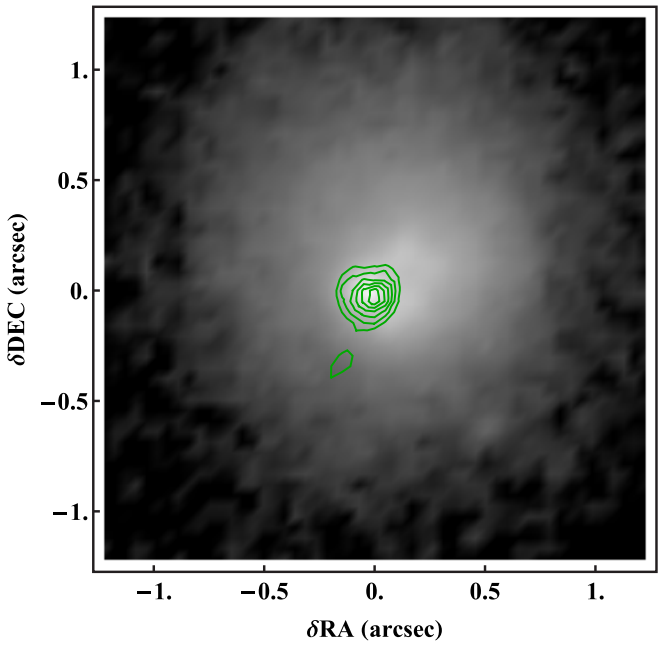

Figure 5. Position of SN2006aj supernova (green contours) within the host galaxy (gray-scale intensity plot) from *HST*/ACS observations in the red F814W band. The supernova position is consistent with the center of the host. The supernova image is computed as the subtraction of the late-time (2006 November 26) image from the early-time (2006 July 18) image. The late-time image without supernova subtraction is taken to represent the host galaxy, which has an irregular morphology. The subtraction is not performed to avoid oversubtraction of the galactic nucleus were the supernova to happen at the very center.

(A color version of this figure is available in the online journal.)

4.6. Associated Supernova and Host Galaxy

Another challenge to the WD/IMBH tidal disruption model is the associated supernova. As discussed in Section 2, the supernova ejecta mass, $M_{\rm ej} \sim (1\text{–}2)\,M_\odot$, is consistent with the high end of the WD mass distribution. The unbound mass fraction is influenced by the interplay between the energy spread during the tidal disruption and the energy release in the supernova explosion. The outflow velocity of tidal disruption debris is 20×10^3 km s^{-1} for the WD and BH masses estimated above, which is comparable to the typical outflow velocity in a Type Ia supernova (10–20) $\times$ 10^3 km s^{-1} (Wang et al. 2009). Thus, the supernova SN2006aj with an energy release comparable to that of a Type Ia supernova (Khokhlov et al. 1993) can unbind most of the WD material, which then contributes to the supernova ejecta mass. Only a small fraction of debris accretes back onto the BH. The nebular phase of SN2006aj exhibits strong oxygen emission (Mazzali et al. 2007), which is consistent with the ignition of a carbon/oxygen WD.

A supernova explosion accompanying a tidal disruption is expected to be heavily asymmetric. In particular, there could be a velocity shift of supernova lines with respect to the velocities of the host galaxy yet the velocities and the redshift $z \approx 0.033$ were only estimated for the host galaxy (Mirabal et al. 2006; Modjaz et al. 2006) and no measurements of supernova velocities exist.

Since IMBHs are expected to reside in the nuclei of dwarf galaxies, the other major test is the coincidence of the supernova position with the center of the host galaxy. A star formation radius for the GRB060218 host is $R_{80} = 0.55$ kpc (Svensson et al. 2010), which corresponds to a half-light radius $R_{50} \approx 0.45$ kpc. The supernova and the host galaxy were observed with *HST*/ACS at different epochs. Figure 5 shows the position of the supernova (green contours) relative to the intensity plot of the host galaxy at a late time. The host galaxy has a somewhat irregular morphology as can be seen in images from Misra et al. (2011), which complicates finding its center. The uncertainty of center determination is about $dR \lesssim 0.1$ arcsec ≈ 70 pc. The supernova position appears to be consistent with the center to within 0.1 arcsec. The ratio of the uncertainty dR to the half-light radius is $dR/R_{50} < 0.15$, which is much less than a normalized offset $dR/R_{50} = 0.98$ found for a representative set of long GRBs (Bloom et al. 2002). It is very rare for a supernova to randomly occur that close to a galactic center.

The stellar mass of the host galaxy is estimated to be $M_{\rm st} \sim 10^{7.2}\,M_\odot$ (Ferrero et al. 2007). Observations suggest that the bulge mass to the total stellar mass ratio (B/T) of galaxies is within the range 15%–100% (Schramm & Silverman 2013) and $B/T = 15\%$ for the Milky Way (McMillan 2011). Then, extrapolating the $M_{\rm bulge}$–$M_{\rm BH}$ relation (Magorrian et al. 1998; Marconi & Hunt 2003)

$$M_{\rm BH}/M_{\rm bulge} \sim 0.002, \tag{24}$$

to low masses, we get a central BH mass of $M_{\rm BH} \sim (0.5\text{–}3) \times 10^4\,M_\odot$. This estimate, though much less certain, is consistent with two previous estimates based on the thermal emission of the jet and the peak time of the light curve.

4.7. Accretion Flow and Jet Energetics

Let us compute the energetics of the jet for the estimated BH mass. Assuming the supernova does not unbind the gas, the accretion rate onto the BH peaks at

$$\dot{M} \approx 2 \times 10^3\,M_\odot\ {\rm yr}^{-1}, \tag{25}$$

which corresponds to the accretion power $\dot{M}c^2 \approx 1 \times 10^{50}$ erg s^{-1}. Then the Blandford–Znajek jet power is $P_{\rm BZ} \sim 0.01\dot{M}c^2 \sim 1 \times 10^{48}$ erg s^{-1} (McKinney 2005) for the low efficiency associated with simulations initiated with a weak magnetic field. The isotropic equivalent radiation power for the opening angle $\theta = 0.5$ and the ratio $Y = 10$ is $P_{\rm rad,iso} \sim 2 \times 10^{48}$ erg s^{-1}. This is substantially higher than the observed peak isotropic luminosity $P_{\rm obs,iso} = 3 \times 10^{46}$ erg s^{-1}. The discrepancy can be partially explained by a small fraction of WD material falling back onto the BH since the supernova may unbind most of the gas. Other potential explanations include GRB060218 happening substantially off-axis, the WD being mostly unbound in an encounter with a spinning BH (Haas et al. 2012), or the source failing to launch a powerful jet. The latter is especially viable since the source has a very limited amount of time to generate the ordered magnetic field. A poloidal magnetic field 10 times weaker than the equipartition value given by Equation (12) leads to consistent jet energetics. The disk may launch a mildly relativistic outflow by itself via the Blandford–Payne mechanism (Blandford & Payne 1982). An off-axis GRB is inconsistent with the absence of a jet break (Soderberg et al. 2006).

The X-ray emission is dominated by a super-Eddington jet at early times, but the accretion disk may be brighter at late times. Our disruption models have a peak accretion rate of about $\dot{M}_{\rm peak} \approx 2 \times 10^3\,M_\odot$ yr^{-1} at the time 2600 s after disruption (neglecting the effect of the material being blown away by a supernova). Then assuming a $t^{-5/3}$ law we find that the accretion rate decreases to the Eddington value for a standard $\varepsilon = 0.1$ efficiency at $t_{\rm Edd} \sim 1$ yr. As described in Section 4.5, the

accretion rate is expected to follow a shallow $t^{-4/3}$ slope after about $t_x \sim 2 \times 10^4$ s due to the viscous evolution in the disk. Yet, as we will describe below in Section 5.1, when the outer disk boundary diffuses out to be much larger than $\sim 20 R_g$, then the energy transfer between the inner and the outer disk kicks in. The energy from the inner flow unbinds the outer material and the accretion rate onto the BH dramatically decreases. Kumar et al. (2008) derived the temporal dependence of the accretion rate in the RIAF with the energy transfer/convection to be $t^{-4(1+s)/3}$ where the parameter s controls the convection efficiency. The value of s varies from $s = 0$ for no energy transfer up to $s = 1$ for the maximum energy transfer power. Thus the accretion rate may decrease as steeply as $t^{-8/3}$ in the RIAF phase. We will discuss RIAFs with convection in more detail in Section 5.1. The onset of a RIAF with energy transfer may explain the steeper XRT flux dependence $F \propto t^{-1.55}$ at times $t > 2 \times 10^5$ s, accompanied by a nearly constant hardness ratio. Therefore, the accretion rate may fall below the Eddington rate at times $t \ll 1$ yr.

The Eddington luminosity for a $2 \times 10^4\ M_\odot$ BH corresponds to a flux

$$F_{\rm Edd} \approx 1 \times 10^{-12}\ {\rm erg\ s^{-1}\ cm^{-2}}, \quad (26)$$

which is about a factor of 100 higher than the late-time flux observed by the XRT. This is not a contradiction, however, as at times much before 1 yr the accretion disk might not be visible at all due to obscuration by the outflowing debris. As discussed in our previous paper (Haas et al. 2012), the outflowing debris consisting of carbon and oxygen has a high absorption cross-section $\sigma \approx 2 \times 10^{-20}$ cm^{-2} across the 0.5–10 keV band. The observed matter velocity in SN2006aj is about 1.5×10^4 km s^{-1} (Mazzali et al. 2006a). A tidal disruption may scatter matter in particular directions, leaving huge voids through which the inner disk could be observed. A tidal disruption of an object with a size comparable to the tidal radius rather tends to scatter the debris over a large solid angle (Haas et al. 2012). In addition, the supernova, whose energy release is comparable to the energy release in a tidal disruption, should scatter the debris more uniformly in all directions. Following Haas et al. (2012), we find that the absorption optical depth unity $\tau = 1$ is achieved around $t \sim 3$ yr, at which time the source is expected to rebrighten. As the accretion disk should have a substantially sub-Eddington accretion rate by 3 yr, the emitted flux level $F_X \lesssim 10^{-13}$ erg s^{-1} cm^{-2}. An accretion flow with a sub-Eddington accretion rate settles into a thin disk (Shakura & Sunyaev 1973), which has an inner temperature of about

$$T_{\rm in} \approx \left(\frac{G M_{\rm BH} \dot{M}}{\sigma_F R_{\rm ISCO}^3} \right)^{1/4}. \quad (27)$$

The temperature is $T_{\rm in} \approx 0.15$ keV for an accretion rate equal to 10% of the Eddington value and a BH mass $2 \times 10^4\ M_\odot$. A very soft blackbody spectrum absorbed by the galactic column and the host galaxy column leads to the ratio $F_{\rm unabs}/F_{\rm abs} \sim 10$ of the model flux to the observed absorbed flux and the observed flux $F_{\rm abs} \sim 10^{-14}$ erg s^{-1} cm^{-2}, which might not be detectable. If rebrightening occurs earlier, while the disk is still radiation dominated and geometrically thick, then the expected observed temperature of the slim disk spectrum is $T_{\rm slim} \approx 0.6$ keV (Haas et al. 2012). Most of the slim disk emission would lie in X-rays, with only an under 1% contribution from the optical/UV at photon energies below 10 eV. A possibility that the disk dominates the emission starting as early as 10^4 s, at which point the source flux equals the Eddington flux of a hypothesized IMBH, is unrealistic. The observed X-ray flux $F_X \sim 10^{-11}$ erg s^{-1} cm^{-2} and the dereddened optical/UV fluxes $F_{\rm opt/UV} \sim 10^{-11}$ erg s^{-1} cm^{-2} (Ghisellini et al. 2007a) are substantially super-Eddington according to Equation (26).

5. EVENT RATES

IMBHs are thought to reside in either the GCs or dwarf galaxies. As we discussed in an earlier work (Haas et al. 2012), the disruption rate of stars by IMBHs in GCs is very uncertain. Baumgardt et al. (2004) predict that for a GC with a $10^3\ M_\odot$ central IMBH, the optimistic disruption rate of stars is 10^{-7} yr^{-1} per GC, while 15% of all disruptions are those of WDs. Thus, following McLaughlin (1999) we theoretically estimate the space density of the GCs to be

$$n_{\rm GC,th} \approx 34\ {\rm Mpc^{-3}}, \quad (28)$$

which leads to a rate of $R_{\rm WD-IMBH} \sim 500$ yr^{-1} Gpc^{-3} of WD disruptions by IMBHs (Haas et al. 2012). Observational constraints on the GC population suggest a slightly lower space density for GCs (Brodie & Strader 2006; Ramirez-Ruiz & Rosswog 2009)

$$n_{\rm GC,obs} \approx 4\ {\rm Mpc^{-3}}, \quad (29)$$

so that the rate estimate should be revised down to

$$R_{\rm WD-IMBH} \sim 50\ {\rm yr^{-1}\ Gpc^{-3}}. \quad (30)$$

The disruption rate of stars in dwarf galaxies was estimated to be very high. If the M–σ (Gebhardt et al. 2000) and $M_{\rm BH}$–$M_{\rm bulge}$ (Magorrian et al. 1998; Marconi & Hunt 2003) relations hold down to low BH masses, then the predicted tidal disruption rate is higher for dwarf galaxies compared to other galaxies (Wang & Merritt 2004). Dependent on the radial stellar profile the disruption rate in a dwarf galaxy with a $10^4\ M_\odot$ BH varies from $R_{\rm IMBH} = 10^{-5}$ yr^{-1} per galaxy up to $R_{\rm IMBH} = 10^{-1}$ yr^{-1} per galaxy. For an estimate we take the rate of $R_{\rm IMBH} = 10^{-3}$ yr^{-1} per galaxy. Note that during a tidal disruption some fraction f of a WD accretes onto a BH. Thus the mass of an IMBH grows at a rate of

$$\frac{dM_{\rm BH}}{dt} = f R_{\rm IMBH} m_{\rm WD}. \quad (31)$$

Taking a large fiducial fraction $f = 0.5$, we find that the BH mass doubles every $t_d = 2 \times 10^8$ yr solely due to tidal disruptions of WDs, where we assumed that the same $R_{\rm WD-IMBH}/R_{\rm IMBH} = 15\%$ of the disrupted stars are WDs. This doubling is consistent with the estimated age of the GRB060218 host galaxy of 200 Myr (Ferrero et al. 2007). As we will show in the next subsection, an IMBH swallows only a small fraction of a MS star so that the IMBH mass growth rate due to MS stars may not be dominant.

According to observations (Ferguson & Sandage 1991), the number density of dwarf (d) galaxies with V magnitude, $M_V > -15.5$, is about the same as the number density of large elliptical (E) and spiral (S) galaxies. Thus, the space density of dwarf galaxies is $n_{\rm dwarf} \sim 10^{-2}$ Mpc^{-3}. Assuming that every dwarf galaxy has a small enough IMBH, we arrive at a rate estimate

$$R_{\rm WD-IMBH} \sim 1500\ {\rm yr^{-1}\ Gpc^{-3}}, \quad (32)$$

which is much larger than the rate in GCs. One event per year for a field of view (FOV) of 10% of the sky would happen as close as 200 Mpc. Such disruptions should be detected by *Swift*

BAT with a FOV of approximately 10% of the sky. Collimation into a wide jet outflow may reduce the rate down to one event per several years consistently with a single GRB060218 source at 143 Mpc distance.

Since WD disruptions by IMBHs produce supernovae, we can compare their rates of occurrence with total supernova rates. Li et al. (2011) found the local rate of Type Ia supernovae to be

$$R_{\rm SN,Ia} \approx 3 \times 10^4 \ {\rm yr}^{-1} \ {\rm Gpc}^{-3}, \quad (33)$$

and the rate of Type Ib/c supernovae to be $R_{\rm SN,Ibc} \approx 3 \times 10^4$ yr^{-1} Gpc^{-3}. In an optimistic estimate, if a supernova is produced in every tidal disruption of a WD, then one disruption-induced supernova happens per 20 Type Ia supernovae. A distinctive feature of disruption-induced supernovae is their location in the galactic nuclei, which is substantially close to the photometric centers of their host dwarf galaxies. This rate equals the rate of calcium-rich gap transients whose properties may be explained by the underluminous explosions of WDs (Kasliwal et al. 2012). However, these transients occur very far from the galactic nuclei.

5.1. Disruptions of MS Stars by IMBHs

In the present paper, we consider radiative signatures of WD disruptions by IMBHs. However, the disruption rates of MS stars by IMBHs are several times higher. The question arises as to whether these more frequent events can produce equally distinct and observable signatures. In this subsection, we show that MS star/IMBH disruptions are quite different from WD/IMBH disruptions: they are much longer and much fainter. Despite their lower rate of occurrence, it might be easier to observe WD/IMBH disruptions compared to MS star/IMBH disruptions.

The fallback timescale is about $t_{\rm fb} \sim 20$ days for a disruption of a 1 $M_\odot$ MS star with solar radius by a 10^4 $M_\odot$ IMBH with a pericenter radius equal to the tidal radius $R_P = R_T$. The peak fallback rate is $\dot{M}_{\rm peak} \sim 5 \, M_\odot$ yr^{-1}. While the tidal disruption radius is $R_T \sim 20 R_{\rm g}$ for a WD, a MS star with solar mass and solar radius has a much larger $R_T \sim 1000 R_{\rm g}$. Since the peak fallback accretion rate $\dot{M}_{\rm peak} \sim 5 \, M_\odot$ yr^{-1} is far above the Eddington rate $\dot{M}_{\rm Edd} \sim 2 \times 10^{-4} \, M_\odot$ yr^{-1}, the RIAF settles from the outer disk radius $R_{\rm disk} \approx 2 R_P$ down to the BH. A RIAF with an outer radius greater than about $20 R_{\rm g}$ settles into a convection-dominated accretion flow (CDAF; Narayan et al. 2000; Quataert & Gruzinov 2000) where the energy transport between the inner and the outer flow starts to play a role. Unlike the fallback disks following WD disruptions, the disks following the disruptions of MS stars always exist in a CDAF state. A flow with convection has a shallow density profile $\rho \propto r^{-\beta}$ down to the inner radius $R_{\rm in} \sim 20 R_{\rm g}$ (Abramowicz et al. 2002). Only a small fraction of available matter accretes in the CDAF state. The sustained BH accretion rate is

$$\dot{M} = \dot{M}_{\rm fb} (R_{\rm disk}/R_{\rm in})^{1.5-\beta}. \quad (34)$$

A density slope of $\beta = 1.5 - s = 0.5$–1.0 was found in numerical simulations (see Yuan et al. 2012 for the review). A value of $\beta = 0.8$–0.9 was estimated by Shcherbakov et al. (2012) for Sgr A*. The flow settles on a viscous timescale $t_{\rm visc} \sim 1$ day, which is shorter than $t_{\rm fb} \sim 20$ days. Thus, the peak accretion rate of the CDAF is given by formula (34) with $\dot{M}_{\rm fb} = \dot{M}_{\rm fb,peak}$. The peak accretion rate onto the BH can be a factor of 10–100 lower than the peak fallback rate

$$\dot{M}_{\rm peak} \sim (0.01\text{–}0.1) \dot{M}_{\rm fb,peak}. \quad (35)$$

Let us make a fiducial estimate for a BH mass of $10^4 \, M_\odot$ and disruption of a Sun-like star for $R_P = R_T$ assuming a density slope of $\beta = 0.85$. In this case the accretion rate is lowered by a factor of $\approx$23 due to the action of convection according to formula (34), and the resultant jet power is $L_{\rm kin} = 0.01 \, \dot{M}_{\rm peak} c^2 \sim 10^{44}$ erg s^{-1} with the same fiducial efficiency $P_0 \sim 0.01$ used in the estimates for WD disruptions. A jet with such low power has a photospheric radius smaller than the saturation radius. The radiation decouples from matter before the jet can accelerate, and powerful photospheric emission is not expected. The photospheric radius corresponds to a bulk Lorentz factor of $\Gamma \approx 2$. If the source is beamed toward us, then the observed temperature is $T_{\rm ob} \approx 0.5$ keV. The radiated blackbody luminosity is $L_{\rm BB} \sim 1 \times 10^{43}$ erg s^{-1}, which corresponds to a distance $d \sim 10$ Mpc to match the peak flux level $F_{\rm peak} \approx 10^{-8}$ erg s^{-1} cm^{-2} of GRB060218. The absorption by the cooled down jet exhaust or a dense wind, which consist mostly of hydrogen and helium, may substantially lower the X-ray luminosity and turn the source into an optical/UV transient similar to the disruption of a MS star by a SMBH (Strubbe & Quataert 2009; Strubbe & Quataert 2011). Optical/UV transients lasting for 20 days and releasing up to 10^{49} erg s^{-1} may be confused with the variability of AGNs. According to the standard theory (Cannizzo & Gehrels 2009; Cannizzo et al. 2011), at $t_x \sim 100$ days the source should switch from the fallback-dominated $t^{-5/3}$ behavior to the disk spreading behavior $t^{-4(1+s)/3} \propto t^{-2.2}$. Yet, a timescale t_x was derived for the adiabatic RIAFs. The temporal behavior of radiatively inefficient fallback accretion disks with convection were not explored to our knowledge and should be investigated in future work. If absorption is inefficient, then one transient per year is expected at a distance $d \sim 100$ Mpc with a peak flux level of about $F_{\rm peak} \approx 10^{-10}$ erg s^{-1} cm^{-2}. Searches within the existing and future X-ray and optical surveys should identify such sources and constrain the rates of tidal disruptions of various kinds. A ROSAT All-Sky Survey search revealed several nearby tidal disruption candidates with redshifts $z \lesssim 0.1$ (Komossa 2002). Some of those candidates, e.g., RX J1242-1119, cannot be easily matched with a large host galaxy (Komossa & Greiner 1999; Komossa et al. 2004). The absence of suitable X-ray/optical transients in the data might not immediately invalidate high tidal disruption rates. For example, if the jet power in disruptions of MS stars is as weak as in GRB060218, then the X-ray/optical flux from such disruptions is expected to be up to 100 times lower. A detailed analysis of tidal disruptions of MS stars is beyond the scope of this paper.

A candidate source for a stellar disruption by an IMBH is a source in GC NGC 1399 explored by Irwin et al. (2010). Observed at a distance of 20 Mpc, the source exhibited an X-ray luminosity of 2×10^{39} erg s^{-1} and a luminosity of a few $\times 10^{36}$ erg s^{-1} in oxygen and nitrogen optical lines. These properties were found to be consistent with disruption of a horizontal branch star by a 50–100 $M_\odot$ BH (Clausen et al. 2012).

6. DISCUSSION AND CONCLUSIONS

In this paper, we explore the theory of WD tidal disruptions by IMBHs, an understudied but very promising type of encounter. The high rate of WD tidal disruptions in dwarf galaxies warrants a search for candidates among already observed objects. We identify GRB060218 with its accompanying supernova, SN2006aj, as a promising candidate and model its temporal/spectral properties and the properties of the host

galaxy. GRB060218 was explored previously within the supernova shock breakout model and the model where a jet is launched by a newborn BH or a neutron star. We find a tidal disruption model to be a viable alternative because it more naturally explains some features of the candidate. In this section, we briefly discuss the application of the tidal disruption model to GRB060218/SN2006aj, and compare different models of the source.

The tidal disruption model performs equally well compared to other models in terms of event rates. The appearance of GRB060218 at a redshift $z = 0.033$ is consistent with a disruption rate of 10^{-3} yr^{-1} of all stars in a dwarf galaxy. The rate of low-luminosity GRBs such as our source was estimated to be about 10% of the Type Ib/c supernova rate (Toma et al. 2007). A number of shock breakouts were observed to accompany supernovae at all distances (Woosley et al. 1999; Mazzali et al. 2006b; Chevalier & Fransson 2008; Schawinski et al. 2008), and the sample of shock breakouts is likely incomplete.

The long emission duration of 2600 s provides a mass estimate of $1 \times 10^4\ M_\odot$ for an IMBH within a tidal disruption scenario. The relativistic shock breakout model also explains the event duration (Nakar & Sari 2012). The extreme smoothness of the spectrum is consistent with either a supernova shock breakout or a jet launched by an IMBH. The jet launched by a stellar mass central object may produce more time variability.

While the observed absorbed X-ray light curve of the event can be fitted with exponential decay within a shock breakout model (Campana et al. 2006), the source flux corrected for absorption exhibits $(t - t_0)^{-5/3}$ behavior specific to the tidal disruptions. Moreover, the full soft X-ray light curve including the rise and decay phases can be fitted well with the accretion rate temporal dependence $\dot{M}(t)$ for a tidal disruption. The steep flux decay at ~6500 s can be ascribed to the source being more heavily absorbed at late times while the jet power and the radiation power still scale as $t^{-5/3}$. Power-law decay is not expected in a shock breakout, while a shallower temporal slope is expected for a jet-powered source (Soderberg et al. 2006). The temporal slope of the afterglow phase, powered by the central engine, is consistent with the accretion rate temporal dependence $t^{-4/3}$ in a RIAF dominated by disk evolution behavior.

The observed blackbody flux and the blackbody temperature can be readily modeled by the jet photospheric emission to provide estimates for the IMBH mass of $1 \times 10^4\ M_\odot$ and for the Lorentz factor of $\Gamma \sim 3$. Moreover, these estimates stay consistent between different time slices in our time-resolved spectroscopic analysis. The rise of the blackbody temperature accompanied by a constant blackbody flux and a decreasing total flux leads to the same BH mass and Lorentz factor over many time slices within the fireball model. The relativistic shock in the wind region of a WR star is able to reproduce the spectrum (Waxman et al. 2007). However, the properties of the underlying WR star and its wind would be peculiar (Li 2007).

The absence of a jet break is consistent with the wide outflow produced without pressure support from the surrounding star. Both the supernova shock breakout and the tidal disruption scenario produce wide outflows.

Strong early optical/UV emission is consistent with coming from the jet front. The non-relativistic outer shells producing early optical/UV blackbody emission violate the source energetics (Ghisellini et al. 2007b) within the supernova shock breakout model. In addition, the total radiated energy $10^{49.5}$ erg of GRB060218 is somewhat higher than expected for shock breakouts (Colgate 1974) in general.

The host of GRB060218 is a dwarf galaxy, and dwarf galaxies are expected to have the highest tidal disruption rates. Only dwarf galaxies (not larger ones) are expected to have IMBHs in their nuclei, and thus disrupt WDs. We crudely estimate a central BH mass of $1 \times 10^4\ M_\odot$ based on the stellar mass of $10^{7.2}\ M_\odot$ of the host. The supernova position is consistent with the center of the host dwarf galaxy, as it should be for a tidal disruption scenario. Supernovae unrelated to the central BHs generally have large displacements from the galactic centers. The supernova SN2006aj has a low estimated ejecta mass $M_{\rm ej} = 1$–$2\ M_\odot$ consistent with a heavy WD.

In sum, the tidal disruption model can explain all features of the source and only the scale of the jet power remains somewhat arbitrary. Note that a BH mass of $1 \times 10^4\ M_\odot$ is estimated in three entirely independent ways! A conclusion that GRB060218 was a tidal disruption by an IMBH in the nucleus of a dwarf galaxy at a distance of 150 Mpc indicates that IMBHs are abundant in the local Universe.

The authors are thankful to Nathaniel Bulter, John Cannizzo, Coleman Miller, Ramesh Narayan, Eve Ostriker, Enrico Ramirez-Ruiz, and Leslie Sage for useful discussions and comments. Special thanks to Abderahmen Zoghbi for advice on temporal analysis, Ranjan Vasudevan for general help with XSPEC, and Demosthenes Kazanas and Jonathan McKinney for discussions of the generation of a large-scale magnetic field. We thank the anonymous referee for insightful comments which helped to improve the manuscript. R.V.S. is supported by NASA Hubble Fellowship grant HST-HF-51298.01, P.L. is supported by NSF grants 1212433, 1205864, 0941417, 0903973, 0855423, and 0903973. C.S.R. thanks NASA for support under Astrophysics Theory Program (ATP) grant NNX10AE41G.

REFERENCES

Abramowicz, M. A., Czerny, B., Lasota, J. P., & Szuszkiewicz, E. 1988, ApJ, 332, 646
Abramowicz, M. A., Igumenshchev, I. V., Quataert, E., & Narayan, R. 2002, ApJ, 565, 1101
Angel, J. R. P. 1978, ARA&A, 16, 487
Arnaud, K. A. 1996, in ASP Conf. Ser. 101, Astronomical Data Analysis Software and Systems V, ed. G. H. Jacoby & J. Barnes (San Francisco, CA: ASP), 17
Balbus, S. A., & Hawley, J. F. 1991, ApJ, 376, 214
Balbus, S. A., & Hawley, J. F. 1998, RvMP, 70, 1
Bardeen, J. M., Press, W. H., & Teukolsky, S. A. 1972, ApJ, 178, 347
Baumgardt, H., Makino, J., & Ebisuzaki, T. 2004, ApJ, 613, 1143
Begelman, M. C., Volonteri, M., & Rees, M. J. 2006, MNRAS, 370, 289
Beloborodov, A. M. 2011, ApJ, 737, 68
Blandford, R. D., & Payne, D. G. 1982, MNRAS, 199, 883
Blandford, R. D., & Znajek, R. L. 1977, MNRAS, 179, 433
Bloom, J. S., Giannios, D., Metzger, B. D., et al. 2011, Sci, 333, 203
Bloom, J. S., Kulkarni, S. R., & Djorgovski, S. G. 2002, AJ, 123, 1111
Brandenburg, A., & Subramanian, K. 2005, PhR, 417, 1
Brodie, J. P., & Strader, J. 2006, ARA&A, 44, 193
Bromberg, O., Nakar, E., & Piran, T. 2011, ApJL, 739, L55
Bufano, F., Pian, E., Sollerman, J., et al. 2012, ApJ, 753, 67
Burrows, D. N., Kennea, J. A., Ghisellini, G., et al. 2011, Natur, 476, 421
Butler, N. R. 2007, ApJ, 656, 1001
Butler, N. R., Kocevski, D., Bloom, J. S., & Curtis, J. L. 2007, ApJ, 671, 656
Campana, S., Mangano, V., Blustin, A. J., et al. 2006, Natur, 442, 1008
Cannizzo, J. K., & Gehrels, N. 2009, ApJ, 700, 1047
Cannizzo, J. K., Lee, H. M., & Goodman, J. 1990, ApJ, 351, 38
Cannizzo, J. K., Troja, E., & Lodato, G. 2011, ApJ, 742, 32
Chevalier, R. A., & Fransson, C. 2008, ApJL, 683, L135
Clausen, D., Sigurdsson, S., Eracleous, M., & Irwin, J. A. 2012, MNRAS, 424, 1268
Colbert, E. J. M., & Mushotzky, R. F. 1999, ApJ, 519, 89
Colgate, S. A. 1968, CaJPh, 46, 476

Colgate, S. A. 1974, ApJ, 187, 333
Daigne, F., & Mochkovitch, R. 2002, MNRAS, 336, 1271
Dainotti, M. G., Bernardini, M. G., Bianco, C. L., et al. 2007, A&A, 471, L29
Daly, R. A. 2011, MNRAS, 414, 1253
Davis, S. W., Narayan, R., Zhu, Y., et al. 2011, ApJ, 734, 111
Davis, S. W., Stone, J. M., & Pessah, M. E. 2010, ApJ, 713, 52
De Colle, F., Guillochon, J., Naiman, J., & Ramirez-Ruiz, E. 2012, ApJ, 760, 103
Dong, X., Wang, T., Yuan, W., et al. 2007, ApJ, 657, 700
Eichler, D., & Levinson, A. 2000, ApJ, 529, 146
Evans, C. R., & Kochanek, C. S. 1989, ApJL, 346, L13
Fabbiano, G., Schweizer, F., & Mackie, G. 1997, ApJ, 478, 542
Fabbiano, G., Zezas, A., & Murray, S. S. 2001, ApJ, 554, 1035
Fan, Y.-Z., Piran, T., & Xu, D. 2006, JCAP, 09, 013
Ferguson, H. C., & Sandage, A. 1991, AJ, 101, 765
Ferrero, P., Kann, D. A., Zeh, A., et al. 2006, A&A, 457, 857
Ferrero, P., Palazzi, E., Pian, E., & Savaglio, S. 2007, in AIP Conf. Proc. 924, The Multicolored Landscape of Compact Objects and Their Explosive Origins, ed. T. di Salvo, G. L. Israel, L. Piersant, L. Burderi, G. Matt, A. Tornambe, & M. T. Menna (Melville, NY: AIP), 120
Fryer, C. L., Woosley, S. E., & Heger, A. 2001, ApJ, 550, 372
Gebhardt, K., Bender, R., Bower, G., et al. 2000, ApJL, 539, L13
Gebhardt, K., Rich, R. M., & Ho, L. C. 2002, ApJL, 578, L41
Ghisellini, G. 2012, in Gamma-Ray Bursts 2012 Conference (GRB 2012), arXiv:1211.2062
Ghisellini, G., Ghirlanda, G., & Tavecchio, F. 2007a, MNRAS, 382, L77
Ghisellini, G., Ghirlanda, G., & Tavecchio, F. 2007b, MNRAS, 375, L36
Giannios, D. 2006, A&A, 457, 763
Giannios, D. 2012, MNRAS, 422, 3092
Gorosabel, J., Larionov, V., Castro-Tirado, A. J., et al. 2006, A&A, 459, L33
Greene, J. E. 2012, NatCo, 3, 1304
Guillochon, J., & Ramirez-Ruiz, E. 2013, ApJ, 767, 15
Gültekin, K., Miller, M. C., & Hamilton, D. P. 2004, ApJ, 616, 221
Haas, R., Shcherbakov, R. V., Bode, T., & Laguna, P. 2012, ApJ, 749, 117
Irwin, J. A., Brink, T. G., Bregman, J. N., & Roberts, T. P. 2010, ApJL, 712, L1
Jorstad, S. G., Marscher, A. P., Lister, M. L., et al. 2005, AJ, 130, 1418
Kasliwal, M. M., Kulkarni, S. R., Gal-Yam, A., et al. 2012, ApJ, 755, 161
Katz, B., Budnik, R., & Waxman, E. 2010, ApJ, 716, 781
Kesden, M. 2012, PhRvD, 85, 024037
Khokhlov, A., Mueller, E., & Hoeflich, P. 1993, A&A, 270, 223
King, A. R., Pringle, J. E., & Livio, M. 2007, MNRAS, 376, 1740
Komossa, S. 2002, in Lighthouses of the Universe: The Most Luminous Celestial Objects and Their Use for Cosmology, ed. M. Gilfanov, R. Sunyeav, & E. Churazov (Berlin: Springer), 436
Komossa, S., & Greiner, J. 1999, A&A, 349, L45
Komossa, S., Halpern, J., Schartel, N., et al. 2004, ApJL, 603, L17
Krolik, J. H., & Piran, T. 2011, ApJ, 743, 134
Kumar, P., Narayan, R., & Johnson, J. L. 2008, MNRAS, 388, 1729
Laguna, P., Miller, W. A., Zurek, W. H., & Davies, M. B. 1993, ApJL, 410, L83
Levan, A. J., Tanvir, N. R., Cenko, S. B., et al. 2011, Sci, 333, 199
Li, L.-X. 2007, MNRAS, 375, 240
Li, W., Chornock, R., Leaman, J., et al. 2011, MNRAS, 412, 1473
Liang, E.-W., Yi, S.-X., Zhang, J., et al. 2010, ApJ, 725, 2209
Liu, D., Pe'er, A., & Loeb, A. 2012, arXiv:1211.5120
Lodato, G., King, A. R., & Pringle, J. E. 2009, MNRAS, 392, 332
Luminet, J.-P. 1985, AnPh, 10, 101
Luminet, J.-P., & Marck, J.-A. 1985, MNRAS, 212, 57
Luminet, J.-P., & Pichon, B. 1989a, A&A, 209, 103
Luminet, J.-P., & Pichon, B. 1989b, A&A, 209, 85
Lynden-Bell, D., & Pringle, J. E. 1974, MNRAS, 168, 603
Madau, P., & Rees, M. J. 2001, ApJL, 551, L27
Maeda, K., Kawabata, K., Tanaka, M., et al. 2007, ApJL, 658, L5
Magorrian, J., Tremaine, S., Richstone, D., et al. 1998, AJ, 115, 2285
Marconi, A., & Hunt, L. K. 2003, ApJL, 589, L21
Matsumoto, H., Tsuru, T. G., Koyama, K., et al. 2001, ApJL, 547, L25
Mazzali, P. A., Deng, J., Nomoto, K., et al. 2006a, Natur, 442, 1018
Mazzali, P. A., Deng, J., Pian, E., et al. 2006b, ApJ, 645, 1323
Mazzali, P. A., Foley, R. J., Deng, J., et al. 2007, ApJ, 661, 892
Mazzali, P. A., Valenti, S., Della Valle, M., et al. 2008, Sci, 321, 1185
McKinney, J. C. 2005, ApJ, 630, 5
McKinney, J. C., & Blandford, R. D. 2009, MNRAS, 394, L126
McKinney, J. C., Tchekhovskoy, A., & Blandford, R. D. 2012, MNRAS, 423, 3083
McLaughlin, D. E. 1999, AJ, 117, 2398
McMillan, P. J. 2011, MNRAS, 414, 2446
Meszaros, P. 2006, RPPh, 69, 2259
Mészáros, P., & Rees, M. J. 2000, ApJ, 530, 292
Metzger, B. D. 2012, MNRAS, 419, 827
Metzger, B. D., Giannios, D., & Mimica, P. 2012, MNRAS, 420, 3528
Miller-Jones, J. C. A., Fender, R. P., & Nakar, E. 2006, MNRAS, 367, 1432
Mirabal, N., Halpern, J. P., An, D., Thorstensen, J. R., & Terndrup, D. M. 2006, ApJL, 643, L99
Misra, K., Fruchter, A. S., & Nugent, P. 2011, in AIP Conf. Proc. 1358, Gamma Ray Bursts 2010, ed. J. E. McEnery, J. L. Racusin, & N. Gehrels (Melville, NY: AIP), 299
Modjaz, M., Stanek, K. Z., Garnavich, P. M., et al. 2006, ApJL, 645, L21
Nakar, E., & Sari, R. 2012, ApJ, 747, 88
Należyty, M., & Madej, J. 2004, A&A, 420, 507
Narayan, R., Igumenshchev, I. V., & Abramowicz, M. A. 2000, ApJ, 539, 798
Narayan, R., Piran, T., & Kumar, P. 2001, ApJ, 557, 949
Nauenberg, M. 1972, ApJ, 175, 417
Nava, L., Ghirlanda, G., Ghisellini, G., & Firmani, C. 2008, MNRAS, 391, 639
Nishimura, J., Mitsuda, K., & Itoh, M. 1986, PASJ, 38, 819
O'Neill, S. M., Reynolds, C. S., Miller, M. C., & Sorathia, K. A. 2011, ApJ, 736, 107
Papadakis, I. E., & Lawrence, A. 1993, MNRAS, 261, 612
Pe'er, A. 2008, ApJ, 682, 463
Pe'er, A., Mészáros, P., & Rees, M. J. 2005, ApJ, 635, 476
Pe'er, A., Mészáros, P., & Rees, M. J. 2006, ApJ, 642, 995
Pe'er, A., & Ryde, F. 2011, ApJ, 732, 49
Pe'er, A., Ryde, F., Wijers, R. A. M. J., Mészáros, P., & Rees, M. J. 2007, ApJL, 664, L1
Penna, R. F., McKinney, J. C., Narayan, R., et al. 2010, MNRAS, 408, 752
Pian, E., Mazzali, P. A., Masetti, N., et al. 2006, Natur, 442, 1011
Poutanen, J., & Svensson, R. 1996, ApJ, 470, 249
Pushkarev, A. B., Kovalev, Y. Y., Lister, M. L., & Savolainen, T. 2009, A&A, 507, L33
Putney, A. 1999, in ASP Conf. Ser. 169, 11th European Workshop on White Dwarfs, ed. S.-E. Solheim & E. G. Meistas (San Francisco, CA: ASP), 195
Quataert, E., & Gruzinov, A. 2000, ApJ, 539, 809
Quataert, E., & Kasen, D. 2012, MNRAS, 419, L1
Ramirez-Ruiz, E., & Rosswog, S. 2009, ApJL, 697, L77
Rees, M. J. 1984, ARA&A, 22, 471
Rees, M. J., & Meszaros, P. 1994, ApJL, 430, L93
Rees, M. J., & Mészáros, P. 2005, ApJ, 628, 847
Rosswog, S., Ramirez-Ruiz, E., & Hix, R. 2009, ApJ, 695, 404
Rybicki, G. B., & Lightman, A. P. 1979, Radiative Processes in Astrophysics (New York: Wiley)
Sari, R., & Piran, T. 1997, ApJ, 485, 270
Schawinski, K., Justham, S., Wolf, C., et al. 2008, Sci, 321, 223
Schneider, R., Ferrara, A., Natarajan, P., & Omukai, K. 2002, ApJ, 571, 30
Schramm, M., & Silverman, J. D. 2013, ApJ, 767, 13
Shakura, N. I., & Sunyaev, R. A. 1973, A&A, 24, 337
Shapiro, S. L., & Teukolsky, S. A. 1986, Black Holes, White Dwarfs and Neutron Stars: The Physics of Compact Objects (New York: Wiley)
Shcherbakov, R. V., Penna, R. F., & McKinney, J. C. 2012, ApJ, 755, 133
Soderberg, A. M., Berger, E., Page, K. L., et al. 2008, Natur, 453, 469
Soderberg, A. M., Kulkarni, S. R., Nakar, E., et al. 2006, Natur, 442, 1014
Stone, J. M., Hawley, J. F., Gammie, C. F., & Balbus, S. A. 1996, ApJ, 463, 656
Stone, N., Sari, R., & Loeb, A. 2012, arXiv:1210.3374
Strubbe, L. E., & Quataert, E. 2009, MNRAS, 400, 2070
Strubbe, L. E., & Quataert, E. 2011, MNRAS, 415, 168
Svensson, K. M., Levan, A. J., Tanvir, N. R., Fruchter, A. S., & Strolger, L.-G. 2010, MNRAS, 405, 57
Takiwaki, T., Kotake, K., & Sato, K. 2009, ApJ, 691, 1360
Tchekhovskoy, A., Metzger, B. D., Giannios, D., & Kelley, L. Z. 2013, arXiv:1301.1982
Tchekhovskoy, A., Narayan, R., & McKinney, J. C. 2010a, ApJ, 711, 50
Tchekhovskoy, A., Narayan, R., & McKinney, J. C. 2010b, NewA, 15, 749
Tchekhovskoy, A., Narayan, R., & McKinney, J. C. 2011, MNRAS, 418, L79
Titarchuk, L. 1994, ApJ, 434, 313
Toma, K., Ioka, K., Sakamoto, T., & Nakamura, T. 2007, ApJ, 659, 1420
Ulmer, A. 1999, ApJ, 514, 180
Usov, V. V. 1992, Natur, 357, 472
Uzdensky, D. A., & MacFadyen, A. I. 2007, ApJ, 669, 546
Wang, J., & Merritt, D. 2004, ApJ, 600, 149
Wang, X., Filippenko, A. V., Ganeshalingam, M., et al. 2009, ApJL, 699, L139
Waxman, E., Mészáros, P., & Campana, S. 2007, ApJ, 667, 351
Wheeler, J. C., Yi, I., Höflich, P., & Wang, L. 2000, ApJ, 537, 810
Wiersema, K., Savaglio, S., Vreeswijk, P. M., et al. 2007, A&A, 464, 529
Woosley, S. E., Eastman, R. G., & Schmidt, B. P. 1999, ApJ, 516, 788
Yuan, F., Wu, M., & Bu, D. 2012, ApJ, 761, 129
Zauderer, B. A., Berger, E., Soderberg, A. M., et al. 2011, Natur, 476, 425